

Non-Hermitian Localization and Population Biology

David R. Nelson and Nadav M. Shnerb

Lyman Laboratory of Physics, Harvard University, Cambridge, MA 02138

(July 2, 2018)

The time evolution of spatial fluctuations in inhomogeneous d -dimensional biological systems is analyzed. A single species continuous growth model, in which the population disperses via diffusion and convection is considered. Time-independent environmental heterogeneities, such as a random distribution of nutrients or sunlight are modeled by quenched disorder in the growth rate. Linearization of this model of population dynamics shows that the fastest growing localized state dominates in a time proportional to a power of the logarithm of the system size. Using an analogy with a Schrödinger equation subject to a constant imaginary vector potential, we propose a delocalization transition for the steady state of the nonlinear problem at a critical convection threshold separating localized and extended states. In the limit of high convection velocity, the linearized growth problem in d dimensions exhibits singular scaling behavior described by a $(d-1)$ -dimensional generalization of the noisy Burgers' equation, with universal singularities in the density of states associated with disorder averaged eigenvalues near the band edge in the complex plane. The Burgers mapping leads to unusual transverse spreading of convecting delocalized populations.

PACS numbers: 05.70.Ln, 87.22.As, 05.40.+j

I. LOCALIZATION AND POPULATION DYNAMICS

The mathematical analysis of spatial patterns in biological systems has been an object of intensive research for many years [1,2]. Both the dynamics and the equilibrium properties of certain model systems have been worked out in detail. Biological processes, such as the spread of a favored gene, population growth of species, ecological competition and so on, are often a combination of diffusion and convection with some kind of back reaction. These systems are not conservative; both growth and death terms, possibly involving nonlinearities, change the number of individuals involved. A general form of such reaction-diffusion equations is [1]

$$\frac{\partial \mathbf{c}}{\partial t} + (\mathbf{v} \cdot \nabla) \mathbf{c} = \mathbf{f}(\mathbf{c}) + \mathbf{D} \nabla^2 \mathbf{c}, \quad (1.1)$$

where $\mathbf{c}(\mathbf{x}, t)$ is the vector of reactants (e.g., species of bacteria, nutrients, etc.), \mathbf{D} is a matrix of diffusivities, and $\mathbf{f}(\mathbf{c})$ describes the nonlinear reaction kinetics. The conservative term $\mathbf{v} \cdot \nabla \mathbf{c}$ represents a convective flux controlled by a drift velocity \mathbf{v} , such as the flow of water in aqueous media, winds, etc.

Although the literature discussing equations of this type is massive, the effect of spatial inhomogeneities in the underlying medium is relatively unexplored [3]. A disordered substrate may manifest itself in the above formalism as quenched random diffusion constants, stochastic growth and death rates or randomness in the reaction term; it may reflect random concentration of environmental factors such as nutrients or toxins, or an inhomogeneous illumination pattern projected onto, e.g., photosynthetic bacteria.

In this paper we study the effect of such heterogeneities in biological systems. As a model we take one of the simplest situations, the case of a *single* species, described by

population number density $c(\mathbf{x}, t)$, for which the reaction diffusion equation is a straightforward generalization of the Malthus-Verhulst growth model [1]:

$$\frac{\partial c(\mathbf{x}, t)}{\partial t} + \mathbf{v} \cdot \nabla c(\mathbf{x}, t) = D \nabla^2 c(\mathbf{x}, t) + [a + U(\mathbf{x})]c(\mathbf{x}, t) - bc^2(\mathbf{x}, t), \quad (1.2)$$

where $U(\mathbf{x})$ is a zero mean quenched random variable, and we take the convective velocity \mathbf{v} to be constant in space and time.

The homogeneous analog of this equation, without the convection term (i.e., $U(\mathbf{x}) = 0$ and $\mathbf{v} = 0$) was proposed by R. A. Fisher [4] as a model for the spread of a favorable genetic mutation. It is also useful as a description of a population dynamics, for which a is the difference between the linear birth and death rates, D reflects the effect of migration, and the term $-bc^2$ represents some self-limiting process, roughly proportional to the number of pairs of individuals at position \mathbf{x} . In the non-random case $U(\mathbf{x}) \equiv 0$, there are two spatially homogeneous fixed points: an unstable fixed point at $c(\mathbf{x}) \equiv 0$, in which there is no population at all, and stable fixed point at $c^*(\mathbf{x}) \equiv a/b$, where the population saturates to the carrying capacity of the environment. Nonnegative initial configurations evolve smoothly toward the stable fixed point; analysis of the time development of spatial fluctuations in this model reveals that equilibrium can be reached via traveling solitonlike solutions, known as Fisher waves [1,4,5].

It is interesting to consider (1.2) in the context of nucleation and spinodal decomposition. In the absence of convection, we can rewrite Eq. (1.2) as

$$\frac{\partial c}{\partial t} = -D \frac{\delta F}{\delta c}, \quad (1.3)$$

where the potential is:

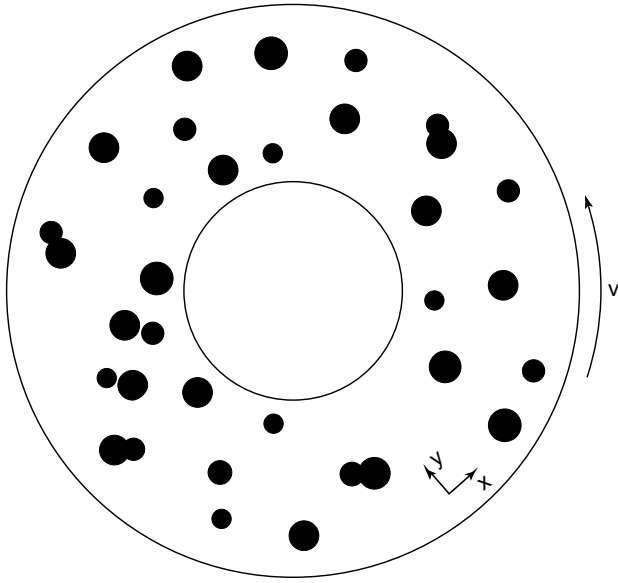


FIG. 1. Schematic of a disordered biological substrate subject to diffusion and convection. The dark spots represent environmental fluctuations, as exemplified by an homogeneous pattern of light projected onto a growing population of bacteria.

$$F(c) = \frac{1}{2}(\nabla c)^2 + \Phi(c) \quad (1.4)$$

with

$$\Phi(c) = -\frac{1}{2D}[a + U(\mathbf{x})]c^2 + \frac{1}{3D}bc^3. \quad (1.5)$$

The time evolution of a small concentration inhomogeneity thus seems to resemble the dynamics of an order parameter quenched below its critical point and subject to a cubic Landau potential $\Phi(c)$ [6]. However, the usual additive Langevin thermal noise term is missing in the dynamics. This reflects the fact that our system admits an absorbing state, i.e., a population state which vanishes everywhere remains fixed at zero. A second crucial difference arises because a smooth nonnegative initial condition will remain nonnegative for all times [7]. The Fisher growth model is thus an unusual zero temperature “one-sided” spinodal decomposition problem. The one-sided nature of the dynamics insures that no unphysical effects arise due to the unbounded potential (1.5) at large negative c . Interesting studies exist of domain growth in, e.g., random Ising systems at zero temperature [8–10], but we are unaware of a similar body of work on “one-sided” population growth models. Another area of active research concerns zero temperature dynamical systems with multiplicative noise [11]. Here, however, the noise typically depends on both space and time, in contrast to the purely space-dependent function $U(\mathbf{x})$ in Eq. (1.2).

In Eq. (1.2), both convection and random fluctuations of the growth rate have been added to the original Fisher model. For the sake of concreteness, we can consider Eq. (1.2) as a model for a colony of bacteria which grows on an inhomogeneous substrate. The linear growth rate of the bacteria depends on a spatially random (but inexhaustible) food supply at each point, or other inhomogeneous, time-independent, environmental factors such as the intensity of illumination. By reducing the light intensity, this linear growth rate could presumably assume both positive and negative values at different points in space. The food or illumination are quenched random variables. The bacteria diffuse, as well as undergo convection due to flow of the ambient medium with velocity \mathbf{v} (Fig. 1) [12].

In this simple model of bacterial population growth, we neglect the dynamics of a diffusing nutrient supply or feedback from waste products [1]. For growth in an inhomogeneous light source, for example, we might require a fixed homogeneous nutrient supply, possibly stabilized by large nutrient diffusion constants. Wakita *et al.* [13] have studied the growth of *Bacillus subtilis* under various conditions, and found a large regime of low Agar density and high nutrient concentration which is well described by the homogeneous analogue of (1.2) without convection, consistent with our assumptions.

If the fluctuating growth rate $U(\mathbf{x})$ is of order δa , we shall see that convection will significantly perturb population growth when the flow rate \mathbf{v} exceeds the corresponding change in the Fisher wave velocity [1] $\delta v_f = 2\sqrt{D\delta a}$. Upon taking as an effective diffusion constant for a motile bacteria $D \sim 6 \times 10^{-6} \text{ cm}^2/\text{sec}$ [14] and growth rate fluctuations $\delta a \sim a = 10^{-3}/\text{sec}$, we find fluctuating Fisher wave velocities of at most a few microns per second. Thus, we shall be primarily concerned with small values of \mathbf{v} and low Reynolds number flows in our analysis.

When randomness is introduced into (1.2), constant configurations are no longer possible steady-state solutions. Instead, the steady state is spatially modulated, reflecting the competition between the disorder and the diffusion term. Convection, on the other hand, tends to make the final state more uniform; For very high convection velocities, one might expect that each bacterium feels some “effective medium” average of the random environment as it drifts rapidly from one site to the other. In this paper, we show that there is a phase transition from one regime to the other in the linearized growth problem and suggest that this sharp change of behavior persists in the steady state.

In order to simplify our problem, let us assume that a stable nonzero steady-state population profile $c^*(\mathbf{x})$, exists, as well as the unstable $c(\mathbf{x}) \equiv 0$ steady state. The time evolution of small fluctuations around these (stable

or unstable) configurations is determined by the linearizing Eq. (1.2) near the fixed point functions. Linearizing about the “Gaussian” fixed point $c(\mathbf{x}) \equiv 0$ leads to

$$\frac{\partial c}{\partial t} \simeq D \nabla^2 c - \mathbf{v} \cdot \nabla c + [a + U(\mathbf{x})]c. \quad (1.6)$$

Linearization about the nontrivial stable steady-state configuration, $c^*(\mathbf{x})$, which satisfies

$$D \nabla^2 c^* - \mathbf{v} \cdot \nabla c^* + [a + U(\mathbf{x})]c^* - 2bc^{*2} = 0, \quad (1.7)$$

leads to a similar equation for $c'(\mathbf{x}, t) \equiv c(\mathbf{x}, t) - c^*(\mathbf{x})$, namely,

$$\frac{\partial c'}{\partial t} \simeq D \nabla^2 c' - \mathbf{v} \cdot \nabla c' + [a + U'(\mathbf{x})]c' \quad (1.8)$$

with

$$U'(\mathbf{x}) = U(\mathbf{x}) - 2bc^*(\mathbf{x}). \quad (1.9)$$

We shall assume that $c^*(\mathbf{x})$ has no long range correlations, so that the linear operator in (1.9) now involves a redefined function $U'(\mathbf{x})$, with quenched random fluctuations away from its mean value similar to those described by $U(\mathbf{x})$.

One main interest in this paper is the evolution of small fluctuations about these fixed point configurations. Near the unstable $c(\mathbf{x}) \equiv 0$ configuration, fluctuations grow until they reach the point for which the linearization fails. On the other hand, small perturbations of the stable state $c^*(\mathbf{x})$ will decay, so that the linear approximation becomes better in time. Thus, Eqs. (1.6) and (1.8), describe the short time growth of dilute populations or the long time decay to the stable state. Although we shall frame most of our discussion in terms of the unstable modes described by (1.6), a very similar analysis applies to Eq. (1.8).

Similar equations emerge in a variety of physical situations, such as models of chemical reactions and neural network [1]. Miller and Wang *et al.* [15] have recently studied the spectrum of an operator describing diffusion of a passive scalar subject to a spatially random, time-independent velocity field, but without simple multiplicative randomness. A closely related physical system from which we intend to draw, is fluctuating vortex lines in superconductors in the presence of columnar defects, with external magnetic field tilted away from the direction parallel to the defects [16,17]. The partition function $\mathcal{Z}(\mathbf{x}, t)$ for a single line at position \mathbf{x} and height t then satisfies Eq. (1.6) where D is given by temperature divided by the tilt modulus, $D = T/(2\tilde{\epsilon}_1)$, \mathbf{v} is proportional to the tilt field, and $U(\mathbf{x})$ corresponds to the columnar disorder potential in the superconductor $V(\mathbf{x})$ normalized by the temperature, $U(\mathbf{x}) = V(\mathbf{x})/T$. Some basic facts about vortex lines are revived in Appendix A. It is interesting to note that Eq. (1.6) also describes the growth of monetary capital with diffusion, spatially varying interest rates and drift due to, say population migration.

Another related problem concerns diffusion and drift of particles in a medium with randomly distributed traps [18–20]. The long time decay of the density of active particles as obtained experimentally from, e.g., photoconduction studies in quasi one dimensional polymers [18], is expected to exhibit stretched exponential relaxation in the absence of a bias [19,20]. When a biasing electric field is present, the decay has a simple exponential prefactor [20] with however a transition from stretched exponential to exponential decay in the subleading behavior above a critical bias threshold [19]. The coarse grained physics can be approximated by Eq. (1.2) without the nonlinearity and $U(\mathbf{x})$ chosen so that *all* growth eigenvalues are negative when $\mathbf{v} = 0$. Our primary concern here is with situations where at least some growth eigenvalues are positive. However, a delocalization transition has also been invoked to describe an abrupt onset of a drift velocity as a function of the bias as the particle density decays in the trapping problem [20]. We discuss the relation of the results of Ref. [19] and [20] to the population biology problem treated here in Appendix C.

After a Cole-Hopf transformation, i.e.,

$$c(\mathbf{x}, t) = \exp[\lambda \Phi(\mathbf{x}, t)], \quad (1.10)$$

the linear growth model described by Eq. (1.6) becomes

$$\begin{aligned} \partial_t \Phi(\mathbf{x}, t) &= D \nabla^2 \Phi(\mathbf{x}, t) + \lambda D (\nabla \Phi)^2 \\ &\quad - \mathbf{v} \cdot \nabla \Phi(\mathbf{x}, t) + a + U(\mathbf{x}), \end{aligned} \quad (1.11)$$

while $c'(\mathbf{x}, t) = \exp[\lambda \Phi'(\mathbf{x}, t)]$ generates a similar equation from Eq. (1.8) with $U(\mathbf{x}) \rightarrow U'(\mathbf{x})$. Chen *et al.* [21] have proposed Eq. (1.11) as a model for the dynamics of strongly driven charge-density waves with quenched disorder. Later in this paper, we use Eq. (1.11) to study sample-to-sample fluctuations in $\ln c(\mathbf{x}, t)$ in the limit of high convection velocities. We obtain exact analytic results, which should be applicable both to linearized models of population dynamics and to charge density waves.

Equations (1.6) and (1.8) may also be written as

$$\partial_t c = \mathcal{L}c, \quad (1.12)$$

where the Liouville operator, e.g.,

$$\mathcal{L} = D \nabla^2 - \mathbf{v} \cdot \nabla + a + U(\mathbf{x}), \quad (1.13)$$

generates the time evolution of the system. The spectra and eigenvalues of random non-Hermitian operators similar to Eq. (1.13) have attracted considerable interest recently [22]. Provided linearization is an adequate approximation, the dynamics of this system is determined by the eigenvalues and the eigenvectors of \mathcal{L} . Near the stable fixed point $c^*(\mathbf{x})$ one expects only decaying modes, i.e., all real parts of the eigenvalue spectrum of \mathcal{L} are negative, while near the unstable state $c(\mathbf{x}) \equiv 0$ there are at least few positive, growing eigenstates. These expectations can be demonstrated explicitly when randomness is absent, i.e., $U(\mathbf{x}) = 0$. In this case the right eigenvectors

of the non-Hermitian operator (1.13) about the unstable fixed point are simple plane waves $\phi_{\mathbf{k}}^R(\mathbf{x}) \sim e^{i\mathbf{k}\cdot\mathbf{x}}$ which satisfy

$$\mathcal{L}\phi_{\mathbf{k}}^R(\mathbf{x}) = \Gamma_{\mathbf{k}}\phi_{\mathbf{k}}^R(\mathbf{x}), \quad (1.14)$$

with the complex eigenvalue spectrum

$$\Gamma(\mathbf{k}) = a - i\mathbf{v} \cdot \mathbf{k} - Dk^2. \quad (1.15)$$

The operator \mathcal{L} which corresponds to linearization about the nontrivial fixed point $c^*(\mathbf{x}) = a/b$ has the same eigenfunctions, with spectrum

$$\Gamma'(\mathbf{k}) = -a - i\mathbf{v} \cdot \mathbf{k} - Dk^2. \quad (1.16)$$

Provided $a > 0$, the eigenvalues of (1.15) have a positive real part for small \mathbf{k} , while all the eigenvalues of (1.16) have a negative real part. Note that the eigenfunctions are always delocalized plane waves.

It is instructive to use the full nonlinear equation (1.2) (with $U(\mathbf{x}) = 0$) to trace the time evolution of a small random initial condition $c(\mathbf{x}, t = 0)$ in terms of the above eigenmodes when $a > 0$. Assume that initial conditions have contributions at all wave vectors \mathbf{k} including $\mathbf{k} = 0$. Although *many* eigenmodes are unstable near $c(\mathbf{x}) \equiv 0$ and grow exponentially in time, the $\mathbf{k} = 0$ mode grows most rapidly. Once this uniform mode saturates at its fixed point value, it then acts to suppress all other growing modes via mode coupling induced by the nonlinear mode coupling term $-bc^2(\mathbf{x}, t)$. These expectations are illustrated via a mean field solution of Eq. (1.2) in Appendix B.

The spatial characteristics of the eigenfunctions of the linearized growth operator change dramatically when randomness is present. When $\mathbf{v} = 0$, the operator $\mathcal{L} = D\nabla^2 + a + U(\mathbf{x})$ is Hermitian with real eigenvalues, and for strong enough disorder, all its eigenfunctions are real and localized; the localization length is smallest in the tails of the energy band, corresponding to extreme values of $U(\mathbf{x})$. In one and two dimensions, it is widely believed that *all* states are localized even for weak disorder [23].

When $\mathbf{v} \neq 0$, the Liouville growth operator is no longer Hermitian, although it can still be diagonalized using a system of left and right eigenvectors. Since the convection term in Eq. (1.6) may be absorbed into the Laplacian by completing the square, $\nabla \rightarrow \nabla + \frac{\mathbf{v}}{2D}$, the right and left eigenfunctions of the new Liouville operator are related to the eigenfunctions of $\mathcal{L}(\mathbf{v} = 0)$ via an imaginary “gauge transformation”; if $\phi_{n,\mathbf{v}=0}(\mathbf{x})$ is an eigenfunction of the Hermitian problem, then [24]

$$\begin{aligned} \phi_{n,\mathbf{v}}^R(\mathbf{x}) &= e^{\mathbf{v}\cdot\mathbf{x}/D} \phi_{n,\mathbf{v}=0}(x) \\ \phi_{n,\mathbf{v}}^L(\mathbf{x}) &= e^{-\mathbf{v}\cdot\mathbf{x}/D} \phi_{n,\mathbf{v}=0}(x) \end{aligned} \quad (1.17)$$

are the eigenfunctions of the non-Hermitian operator with the *same* eigenvalue ϵ_n , up to a constant shift [20],

$$\epsilon_n \rightarrow \epsilon_n(\mathbf{v}) = \epsilon_n(\mathbf{v} = 0) - \frac{v^2}{4D} \quad (1)$$

provided that ξ_n , the localization length in the non-driven problem, is less than D/\mathbf{v} . Thus, for small convection velocities, there is a *spectral rigidity* - except for the shift, the real eigenvalue spectrum is locked to the values it had for $\mathbf{v} = 0$. As \mathbf{v} increases, however, some eigenfunctions eventually become extended and the dynamics becomes sensitive to boundary effects. The correct eigenfunctions and eigenvalues are no longer related to the $\mathbf{v} = 0$ case by a simple transformation. In case of periodic boundary conditions, complex eigenvalues and delocalized modes appear when D/v becomes smaller than ξ_n . As \mathbf{v} is increased, these delocalized states appear first at the band center, for which the localization length is maximal, then move outwards.

These expectations for the eigenvalue spectrum have been demonstrated by analytic work and a numerical analysis of a discrete lattice model, inspired by the physics of vortex lines [25]. The corresponding lattice discretization of the nonlinear equation which motivates our present work reads

$$\begin{aligned} \frac{dc_{\mathbf{x}}(t)}{dt} &= \frac{w}{2} \sum_{\mathbf{x}} \sum_{\nu=1}^d [e^{\mathbf{g}\cdot\mathbf{e}_{\nu}} c_{\mathbf{x}+\mathbf{e}_{\nu}}(t) + e^{-\mathbf{g}\cdot\mathbf{e}_{\nu}} c_{\mathbf{x}-\mathbf{e}_{\nu}}(t)] \\ &+ \sum_{\mathbf{x}} [a + U(\mathbf{x})] c_{\mathbf{x}}(t) - b \sum_{\mathbf{x}} c_{\mathbf{x}}^2(t), \end{aligned} \quad (1.18)$$

where $c_{\mathbf{x}}(t)$ is the species population at the sites $\{\mathbf{x}\}$ of a hypercubic lattice, and the $\{\mathbf{e}_{\nu}\}$ are unit lattice vectors. Here w is proportional to the diffusion constant of the corresponding continuum model ($w \sim D/\ell_0^2$), and \mathbf{g} is proportional to the flow rate \mathbf{v} . Up to subtraction proportional to v^2/D in a , a , $U(\mathbf{x})$ and b have the same interpretation as in the continuum model. When linearized about $c_{\mathbf{x}} \equiv 0$, Eq. (1.18) may be written

$$\frac{dc_{\mathbf{x}}(t)}{dt} = \sum_{\mathbf{x}'} \tilde{\mathcal{L}}(\mathbf{x}, \mathbf{x}') c_{\mathbf{x}'}(t) \quad (1.19)$$

where the discrete Liouville operator $\tilde{\mathcal{L}}$ is the matrix

$$\begin{aligned} \tilde{\mathcal{L}} &= \frac{w}{2} \sum_{\mathbf{x}} \sum_{\nu=1}^d [e^{-\mathbf{g}\cdot\mathbf{e}_{\nu}} |\mathbf{x} + \mathbf{e}_{\nu}\rangle \langle \mathbf{x}| + e^{\mathbf{g}\cdot\mathbf{e}_{\nu}} |\mathbf{x}\rangle \langle \mathbf{x} + \mathbf{e}_{\nu}|] \\ &+ \sum_{\mathbf{x}} [a + U(\mathbf{x})] |\mathbf{x}\rangle \langle \mathbf{x}| \end{aligned} \quad (1.20)$$

As in the continuum case, the same equation arises when linearized about the a nontrivial fixed point $c_{\mathbf{x}}^*$ provided we make the replacement $U(\mathbf{x}) \rightarrow U'(\mathbf{x})$ with $U'(\mathbf{x})$ given by Eq. (1.9)

Typical spectra for a 1000-site model in one dimension with $U(\mathbf{x})$ uniformly distributed in the interval $[-\Delta, \Delta]$ are shown in Fig. 2 for three values of $g \propto v$ [25].

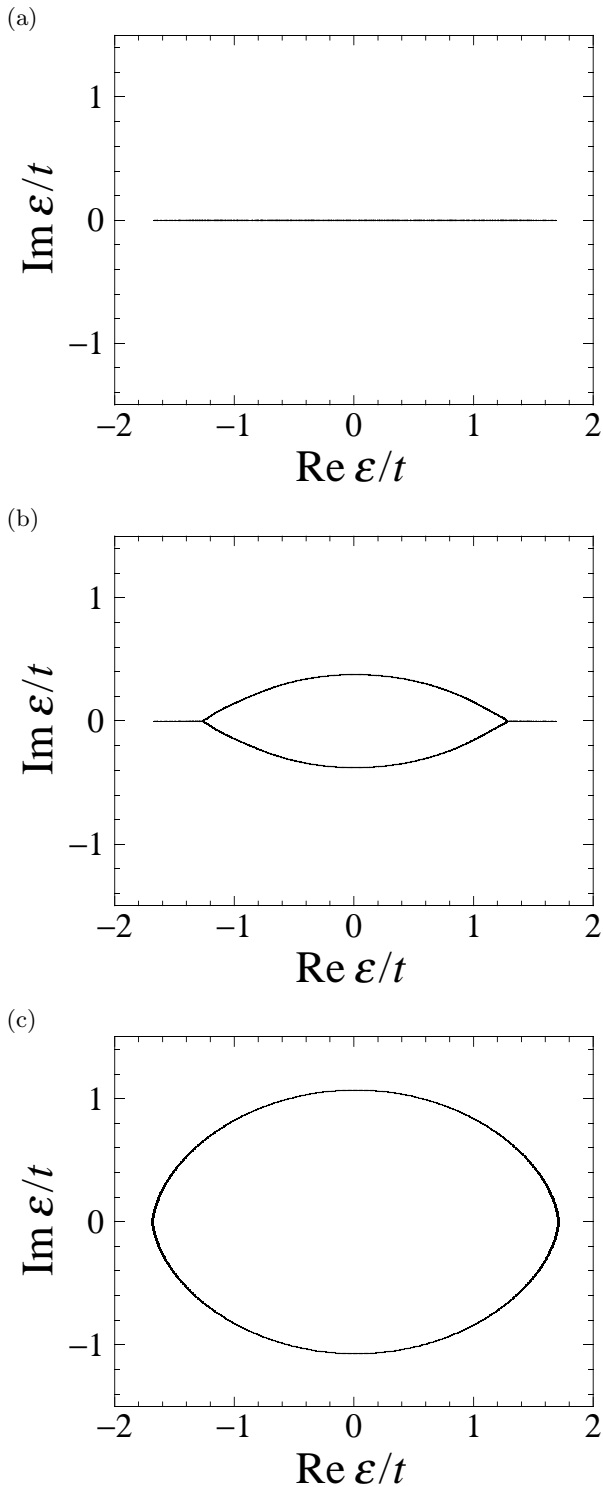


FIG. 2. Energy spectra of one-dimensional 1000-site lattice model with randomness $\Delta/w = 1$. The resulting spectrum for the same realization of the random potential $U(x) \in [-\Delta, \Delta]$ is plotted here for three different values of g . (a) Case $g < g_1$; all eigenstates are localized; (b) $g_1 < g < g_2$; bubble of complex eigenvalues indicating extended states appears near the center of the band; (c) $g_2 < g$; all the eigenstates are extended. (After Ref. [25]).

For g less than a critical value g_1 , all eigenmodes are localized, and the eigenvalues remain real and locked to their values for $g = 0$. For $g_1 < g < g_2$, extended states with complex eigenvalues appear near the center of the band. Localized states still appear near the band edges. For $g > g_2$, every localized state is destroyed by the non-Hermitian perturbation, and all states are extended. In this limit, eigenfunctions are slightly perturbed Bloch states—the lattice version of plane waves. The spectrum is well approximated by the disorder-free limit, i.e., the lattice analogue of Eq. (1.15)

$$\Gamma(k) = 2w \cos(k\ell_0 + ig\ell_0), \quad (1.21)$$

where ℓ_0 is the lattice constant.

With our definition of $\tilde{\mathcal{L}}$, states near the *top* of the band should give a reasonable approximation to the spectrum of the continuous operator (1.14); Eq. (1.15) then describes the upper edge of the ellipse of eigenvalues in Fig. 2c. The states at the bottom of the band, on the other hand, have spatial characteristics which are artifacts of the lattice discretization.

Figure 3 shows typical spectra for the discrete operator in *two* dimensions [25]. Here, too, eigenfunctions near the top of the band should give good approximation to growth modes in the continuum limit. Again, all eigenvalues remain real and the eigenfunctions remain localized when $g < g_1$. For $g_1 < g < g_2$, however, extended and localized states *coexist* near the center of the band [25]. When $g > g_2$, even most rapidly growing states at the top of the band are delocalized. For *very* large g (not shown) the spectrum resembles that of the disorder-free limit of the lattice model, similar to the one-dimensional case. However, as mentioned in Ref. [25], this apparent simplification is actually a finite size artifact in $d = 2$: level repulsion leads to large modification of the Bloch wave functions and eigenvalues even for weak disorder in any sufficiently large system. Thus, chaotic spectra similar to Fig. 3c are always expected for large v due to disorder in the “thermodynamic limit” of large system sizes in $d = 2$. In Sec. 4 we argue that the growth for $g > g_2$ when $d \geq 2$ is in fact described by the $(d - 1)$ -dimensional Schrödinger-like equation with space- and time-dependent randomness. The anomalous critical exponents which describe this situation lead to universal power law singularities in the density of states near the band edge in the complex plane.

If we take a gradient and set $\mathbf{u}(\mathbf{x}, t) = -\nabla\Phi(\mathbf{x}, t)$, the dynamical growth model (1.11) which results from a Cole-Hopf transformation reads

$$\begin{aligned} \partial_t \mathbf{u}(\mathbf{x}, t) + (\mathbf{v} \cdot \nabla) \mathbf{u}(\mathbf{x}, t) + 2\lambda D(\mathbf{u}(\mathbf{x}, t) \cdot \nabla) \mathbf{u}(\mathbf{x}, t) \\ = D \nabla^2 \mathbf{u}(\mathbf{x}, t) + \mathbf{f}(\mathbf{x}), \end{aligned} \quad (1.22)$$

with $\mathbf{f}(\mathbf{x}) = \nabla U(\mathbf{x})$ and subject to the constraint $\nabla \times \mathbf{u} = 0$. This is a variant of the d -dimensional generalization of Burger’s equation with noise studied 20 years ago by Forster *et al.* [26]. In the form (1.11), such problems are sometimes referred to as “KPZ equations”.

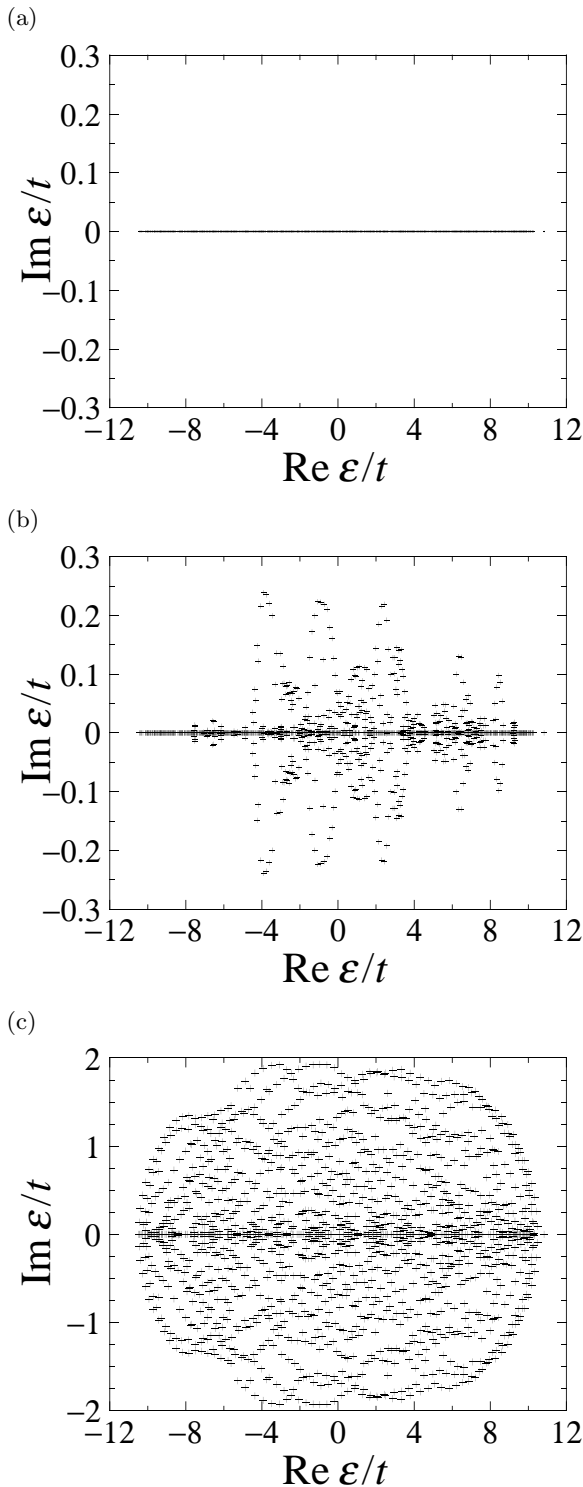


FIG. 3. Typical spectra of the two-dimensional tight-binding non-Hermitian model with random site potential. (a) Case $g < g_1$; delocalized states, real spectrum. (b) $g_1 < g < g_2$; extended states with complex eigenvalues coexist with localized states with real eigenvalues near the center of the band. (c) $g_2 < g$; states at the tails of the band become extended, and there are complex eigenvalues even near the top of the band. (After Ref. [25].)

In Sec. 5, we show that (1.22) is in the same universality class as a simpler $(d-1)$ -dimensional noisy Burgers' equation, and use this fact to study sample-to-sample fluctuations of $\ln[c(\mathbf{x}, t)]$ for large v . Thus, as the convective velocity \mathbf{v} grows from small toward large values, the most rapidly growing modes evolve from a dynamics described by Anderson localization into a regime related to the Burgers' model for turbulence [27].

The remainder of this paper is organized as follows. In Sec. 2, we assume convective effects are small, and illustrate the consequences of localization for “unbounded” population growth, i.e., growth at times before the nonlinear term in Eq. (1.2) becomes important. In Sec. 3, we describe how these nonlinearities affect the growth when only a few modes are unstable relative to the state $c(\mathbf{x}) \equiv 0$. Unlike growth in a homogeneous environment, the most rapidly growing eigenfunction does not suppress all other unstable modes in this case. We suggest that the steady state undergoes a delocalization transition which occurs when the average growth rate or the convective velocity \mathbf{v} are increased.

In Sec. 4, we study the linearized growth problem in the large v limit, show that the physics is related to a $(d-1)$ -dimensional Schrödinger equation and demonstrate that the average growth spectrum is singular for $d \geq 2$. This mapping leads to *universal* predictions for the randomness-dominated transverse wandering of a delocalized population as it drifts downstream. A $d-1$ -dimensional Burgers' equation is used to describe sample to sample fluctuations in $\ln[c(\mathbf{x}, t)]$ in the limit of large \mathbf{v} in Section 5. A number of related calculations are contained in three Appendices. Appendix C contains a discussion of the stretched exponential relaxation expected for populations in a medium with randomly distributed traps.

II. UNBOUNDED GROWTH AND THE LOCALIZED LIMIT

There is large literature on localization of electrons in disordered semiconductors [23]. Because the linearized growth modes which arise from Eq. (1.2) obey a Schrödinger-like equation, one might hope that results from electron localization theory would be applicable to the simple model of heterogeneous population dynamics discussed above. Of course, electronic states are either empty or full, according to Pauli exclusion principle. In contrast, *many* individual members of a species participate in the growth modes determined by the continuum model equation studied here. Another difference is the form of the growth-limiting nonlinearity in Eq. (1.2).

In this section, we explore the consequences of localization for the simple problem of “unbounded growth”, i.e., growth at times before the nonlinearity in Eq. (1.2) becomes important. We assume homogeneous initial conditions, weak convection, and parameters (small b , for example) such that the time domain over which unbounded

growth occurs is very large. Effects of the nonlinear term will be discussed in Sec. 3.

Although many modes may now be growing exponentially, the fastest growing eigenfunction eventually dominates the center of mass of the evolving population distribution. We show here that the time t^* it takes for the “ground state” (i.e., the *fastest* growing eigenfunction) to win out in a large but finite domain grows very slowly as a function of the domain radius R . The precise form of $t^*(R)$ depends on the behavior of the density of localized states in the tail of the band of growth eigenvalues. For the simple discretized growth model discussed in Sec. 1, $t^*(R) \sim \ln^{2/d}(R)$ where d is the dimensionality of space. Comparable results in semiconductors are usually determined by electrons at Fermi energy in a partially filled band, and hence are less sensitive to the form of the density of states. The time required for ground state dominance when populations grow in a spatially homogeneous environment is very different, $t^*(R) \sim R^2$.

Given a time-independent Liouville operator \mathcal{L} , as in Eq. (1.13), we describe growth in terms of a complete set of left and right eigenvectors $\{\phi_n^L(\mathbf{x})\}$ and $\{\phi_n^R(\mathbf{x})\}$, with eigenvalues $\{\Gamma_n\}$ (the complex “energy spectrum”). The time evolution of $c(\mathbf{x}, t)$ is then given by

$$c(\mathbf{x}, t) = \sum_n c_n \phi_n^R(\mathbf{x}) e^{\Gamma_n t} \quad (2.1)$$

where the coefficients $\{c_n\}$ are determined by the initial condition,

$$c_n = \int d^d \mathbf{x} \phi_n^L(\mathbf{x}) c(\mathbf{x}, t=0) \quad (2.2)$$

At long times the system will be dominated by the “ground state”, i.e., the state for which the real part Γ_n is *maximal*. Throughout this paper, we assume that there is such a state, i.e., that the real part of the spectrum is bounded above. The Liouville operator in Eq. (1.13) plays, with the replacement $t \rightarrow -it$ and $\mathcal{L} \rightarrow -\mathcal{H}$ a role similar to the Hamiltonian \mathcal{H} in the Schrödinger equation $i\hbar \partial_t c = \mathcal{H}c$. We shall often use nomenclature from quantum mechanics, such as “energy spectrum” and “low-lying states”. However, because of the identification $\mathcal{H} \equiv -\mathcal{L}$, the ground state of the Hamiltonian is actually the state with the *maximal* eigenvalue of the Liouville operator, and the low-lying states of the Hamiltonian are those which grow fastest for the Liouville operator.

We assume a small convective velocity, so that the left and right eigenfunctions are described by slightly distorted versions of the localized state for $\mathbf{v} = \mathbf{0}$, as in Eq. (1.17), with normalization

$$\int d^d \mathbf{x} \phi_m^L(\mathbf{x}) \phi_n^R(\mathbf{x}) = \delta_{m,n}. \quad (2.3)$$

Deep in the band tail and close to the ground state, the n^{th} localized eigenfunction for $\mathbf{v} = \mathbf{0}$ will have the approximate form

$$\phi_{n,\mathbf{v}=0}(\mathbf{x}) \sim b_n e^{-\kappa_n |\mathbf{x} - \mathbf{x}_n|}, \quad (2.4)$$

where $b_n \propto \kappa_n^{d/2}$ is a normalization constant and κ_n is the inverse localization length associated with an eigenmode located at position \mathbf{x}_n .

Of course, only the ground state is guaranteed to be strictly nonnegative [28], as implied by Eq. (2.4). Orthogonality with the ground state requires a small negative part in the localized excited state eigenfunctions. Nevertheless, Eq. (2.4) should be a good approximation

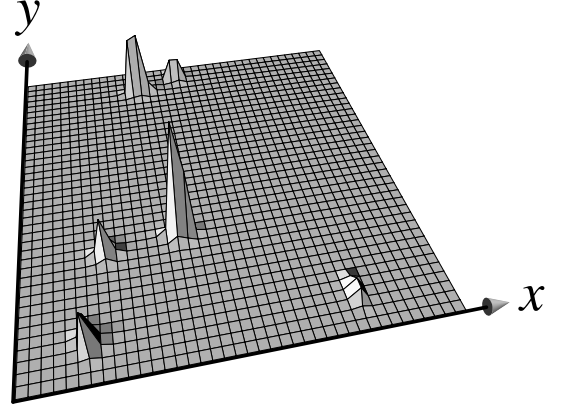


FIG. 4. The six fastest growing localized eigenfunctions for the two-dimensional lattice model (with $v \propto g = 0$) which gave rise to the spectrum of Fig. 3(a). (Figure courtesy of Naomichi Hatano)

for all modes in the tail of the growth spectrum, provided the disorder is strong: Strong disorder means that all states are well localized, with approximately the same localization length. The six fastest growing modes on the square lattice which gave rise to the spectrum in Fig. 3a are shown in Fig. 4.

Suppose the environment has been inoculated with a small *uniform* population of, say, bacteria at time $t = 0$. Then the projections $\{c_n\}$ of this initial condition onto the localized eigenmodes are approximately equal, $c_n \approx c_0$ for all n . The normalized species concentration,

$$\hat{c}(\mathbf{x}, t) = \frac{c(\mathbf{x}, t)}{\int d^d \mathbf{x} c(\mathbf{x}, t)} \quad (2.5)$$

is given by

$$\hat{c}(\mathbf{x}, t) \approx \frac{\phi_{gs}^R(\mathbf{x}) + \sum'_n \phi_n^R(\mathbf{x}) e^{-(\Gamma_{gs} - \Gamma_n)t}}{N_{gs} + \sum'_n N_n e^{-(\Gamma_{gs} - \Gamma_n)t}} \quad (2.6)$$

where N_{gs} and the $\{N_n\}$ are normalization constants,

$$N_{gs} = \int d^d \mathbf{x} \phi_{gs}^R(\mathbf{x}), \quad N_n = \int d^d \mathbf{x} \phi_n^R(\mathbf{x}). \quad (2.7)$$

We have separated out the “ground state,” i.e., the most rapidly growing mode and the sums \sum'_n are over the remaining excited states.

The time necessary for the ground state to dominate the normalized species concentration in a large region of size R is clearly of order $t^* \sim 1/(\Gamma_{gs} - \Gamma_n^*) \equiv 1/\Delta\Gamma$, where Γ_n^* is the growth rate of the first excited state in the region. Let $g(\Gamma)$ be the density of states per unit volume with growth rates in the interval between Γ and $\Gamma + d\Gamma$. Then, as we increase $\Delta\Gamma$ from zero, an excited state with gap $\Delta\Gamma$ will appear when

$$R^d g(\Delta\Gamma) \Delta\Gamma \approx 1. \quad (2.8)$$

If $g(\Delta\Gamma)$ were approximately constant near the band edge, then $\Delta\Gamma \sim 1/R^d$ and we would have $t^*(R) \sim R^d$. However, there are in fact very few states in the tail of a band of localized eigenfunctions [23]. In Appendix C, we show that, for the simple lattice model of population growth discussed in Section 1,

$$\Gamma_{gs} \approx a + wd + \Delta \quad (2.9)$$

and

$$g(\Delta\Gamma) \sim \exp[-(\text{const.}/\Delta\Gamma)^{d/2}] \quad (2.10)$$

as $\Delta\Gamma \rightarrow 0$. Solving Eq. (2.8) for large R now leads to $\Delta\Gamma \sim 1/\ln(R/l_0)^{2/d}$ where l_0 is the lattice constant of the model. The relaxation time for a system of size R is then

$$t^*(R) \sim \ln^{2/d}(R/l_0), \quad \text{localized growth.} \quad (2.11)$$

The sparse population of growth rates near the ground state results in slow logarithmic growth of the relaxation time $t^*(R)$ with system size R . A very different size dependence results for the delocalized modes of the homogeneous model. For delocalized plane wave eigenfunctions described by a spectrum like (1.15), there are many more states close to the ground state. When $\mathbf{v} = 0$ the density of states $g(\Delta\Gamma) \sim (\Delta\Gamma)^{d/2-1}$ near the band edge in the delocalized limit, and the above argument leads to

$$t^*(R) \sim R^2, \quad \text{delocalized growth.} \quad (2.12)$$

III. INTERACTIONS AND A DELOCALIZATION TRANSITION

A complete analysis of the nonlinear “interaction” terms in Eq. (1.2), or its lattice equivalent Eq. (1.18), is beyond the scope of this paper. Some progress is possible, however, when only a few strongly localized growth eigenvalues near the band edge of the Liouville operator have a positive real part. In this limit, it is easy to demonstrate that localized population dynamics with interactions differs considerably from the dynamics of the plane waves which describe population growth in a homogeneous environment. We shall also argue that the sharp mobility edge separating localized eigenfunctions from delocalized

ones [25] implies a delocalization transition with increasing convective velocity or average growth rate in population dynamics. This transition is clearly present in the linearized growth model, and we shall give arguments that it may be present as well in steady-state population distributions described by Eqs. (1.2) and (1.18).

Let us write Eq. (1.2) in the form

$$\frac{\partial c(\mathbf{x}, t)}{\partial t} = \mathcal{L}c(\mathbf{x}, t) - bc^2(\mathbf{x}, t) \quad (3.1)$$

where \mathcal{L} is the Liouville operator (1.13), and study the steady state which develops for long times. Upon expanding in the complete set of right eigenfunctions of \mathcal{L} , with eigenvalues Γ_n

$$c(\mathbf{x}, t) = \sum_n c_n(t) \phi_n^R(\mathbf{x}), \quad (3.2)$$

the dynamical equations read

$$\frac{dc_n(t)}{dt} = \Gamma_n c_n(t) - \sum_{m, m'} w_{n, mm'} c_m(t) c_{m'}(t), \quad (3.3)$$

where the mode coupling coefficients are

$$w_{n, mm'} = b \int d^d \mathbf{x} \phi_n^L(\mathbf{x}) \phi_m^R(\mathbf{x}) \phi_{m'}^R(\mathbf{x}) \quad (3.4)$$

Upon combining the “gauge transformation” Eq. (1.17) with the approximate form (2.4) of the localized eigenfunctions, the orthogonality condition (2.3) leads to [25]

$$\phi_n^R \simeq \sqrt{\frac{(2\kappa_n)^d}{\Gamma(d)\Omega(d)}} \exp[\mathbf{v} \cdot (\mathbf{x} - \mathbf{x}_n)/D - \kappa_n |\mathbf{x} - \mathbf{x}_n|] \quad (3.5)$$

$$\phi_n^L \simeq \sqrt{\frac{(2\kappa_n)^d}{\Gamma(d)\Omega(d)}} \exp[-\mathbf{v} \cdot (\mathbf{x} - \mathbf{x}_n)/D - \kappa_n |\mathbf{x} - \mathbf{x}_n|]$$

where Ω_d is the surface area of a unit sphere in d dimensions.

Now consider what happens in, say, the lattice population growth model (1.18) when we vary the average growth rate a , starting with large negative values. As discussed in Appendix C, the real part of the growth spectrum broadens to a width of order $wd + \Delta$ about a due to diffusive hopping between sites and randomness. If $-a \gg wd + \Delta$, then the real parts of all eigenvalues in Eq. (3.3) are negative and the population becomes extinct. As we increase a however we eventually reach the simple but interesting situation where a small fraction of the eigenvalues become positive. The coupled equations (3.3) then resemble the set of renormalization group recursion relations governing flows in the space of Hamiltonian coupling constants which describe equilibrium critical points to one loop order [29]. Here, an expansion in $\epsilon = 4 - d$ is used to truncate an infinite set

of coupled differential equations. By analogy with critical phenomena, we call the modes with positive $\text{Re}(\Gamma_n)$ “relevant variables” and those with negative $\text{Re}(\Gamma_n)$ “irrelevant variables”. To a first approximation, we can simply discard the irrelevant variables in Eq. (3.3), because their negative eigenvalues are not much affected by the dilute concentration of growing modes (see below), and they will eventually die out.

The behavior of the relevant variables is also simple. Because these constitute only a small fraction of the total number of localized modes, they will be widely separated in space. The overlap integral which defines the coupling coefficients in Eq. (3.5) will then be negligible unless $m = m' = n$ and the differential equations describing the localized eigenmodes decouple,

$$\frac{dc_n(t)}{dt} = \Gamma_n c_n(t) - w_n c_n^2(t) \quad (3.6)$$

where

$$w_n \equiv w_{n,nn} = b \int d^d \mathbf{x} \phi_n^L(\mathbf{x}) [\phi_n^R(\mathbf{x})]^2 \quad (3.7)$$

If the convective velocity is small, the eigenvalues Γ_n remain locked at their values for $\mathbf{v} \propto \mathbf{g} = 0$, and the neglected terms are smaller by a power of $\exp[-\kappa l]$, where l is a typical spacing between relevant eigenmodes.

The evolution of $c(\mathbf{x}, t)$ at long times (after the irrelevant variables have died off) is determined by substituting the solutions of Eq. (3.6),

$$c_n(t) = \frac{c_n(0)e^{\Gamma_n t}}{1 + c_n(0)\frac{w_n}{\Gamma_n}(e^{\Gamma_n t} - 1)}, \quad (3.8)$$

into Eq. (3.2) and only summing over the unstable modes. In contrast to the homogeneous population dynamics, where a *single* $\mathbf{k} = 0$ eigenfunction completely dominates the steady state (see Appendix B), the fastest growing localized eigenfunction does not interact appreciably with the other relevant variables. The steady-state fixed point $c^*(\mathbf{x})$ approached at long times is then characterized by *many* occupied modes,

$$c^*(\mathbf{x}) = \sum_n' c_n^* \phi_n^R(\mathbf{x}) \quad (3.9)$$

where the fixed point values c_n^* are

$$c_n^* = \frac{\Gamma_n}{w_n}, \quad (3.10)$$

and \sum_n' means only unstable eigenfunctions make a nonzero contribution to the sum. This state is similar to the “Bose glass” phase of flux lines in Type II superconductors, where a plays a role of a chemical potential for vortices [17]. Unlike the Bose glass, however, the number of degrees of freedom associated with each occupied localized state is highly variable. The “occupation number” N_n of an unstable eigenmode is, from Eq. (3.9),

$$N_n = c_n^* \int d^d \mathbf{x} \phi_n^R(\mathbf{x}) \quad (3.11)$$

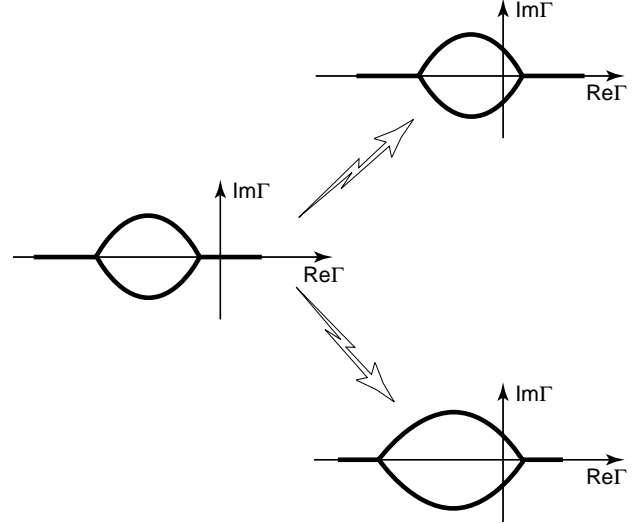


FIG. 5. Schematic of a one-dimensional eigenvalue spectrum below and above the delocalization threshold. On the left, only a few localized states are unstable and the bubble of “irrelevant” delocalized states has little effect on the steady state. Spectra on the right have unstable delocalized states arising either from an increase in the average growth rate a (top) or an increase in the convective velocity v with $a - v^2/4D$ held fixed (bottom).

We checked the above analysis in one dimension for $g \propto v = 0$ by numerically determining the eigenfunctions in Eq. (1.20) for a particular realization of the random potential $U(x) \in [-\Delta, \Delta]$ with a sufficiently negative so that only four eigenvalues on a 700 site lattice were positive. This situation is qualitatively similar to that shown on the left side of Fig. 5, except that there is no bubble of delocalized states in the center of the band for $g = 0$. However, provided $\text{Re}(\Gamma_n)$ is large and negative for these delocalized states, they rapidly die off and will not affect the fixed point describing the steady state. We then determined the steady state population distribution for the full nonlinear equation (1.18) under the same conditions. This steady state is compared with the four relevant eigenmodes of the linearized problem in Fig. 6. The peaks in the exact steady state (top part of the figure) do indeed occur precisely at the locations of the four unstable growth eigenfunctions. It is easy to see from Eq. (3.4) that $w_{n,nn} = \text{const. } \kappa_n^{d/2}$. Since κ_n (the inverse width of the localized eigenfunctions) is approximately independent of n and equal to the lattice constant in the tail of the band (see, e.g., Ref. [25]), it follows from Eq. (3.10) that the *heights* of the peaks in the steady state are proportional to the growth *eigenvalues* of the unstable modes in this simple model of population dynamics. We have checked that this relationship between peak heights and growth rates is satisfied by the steady state of

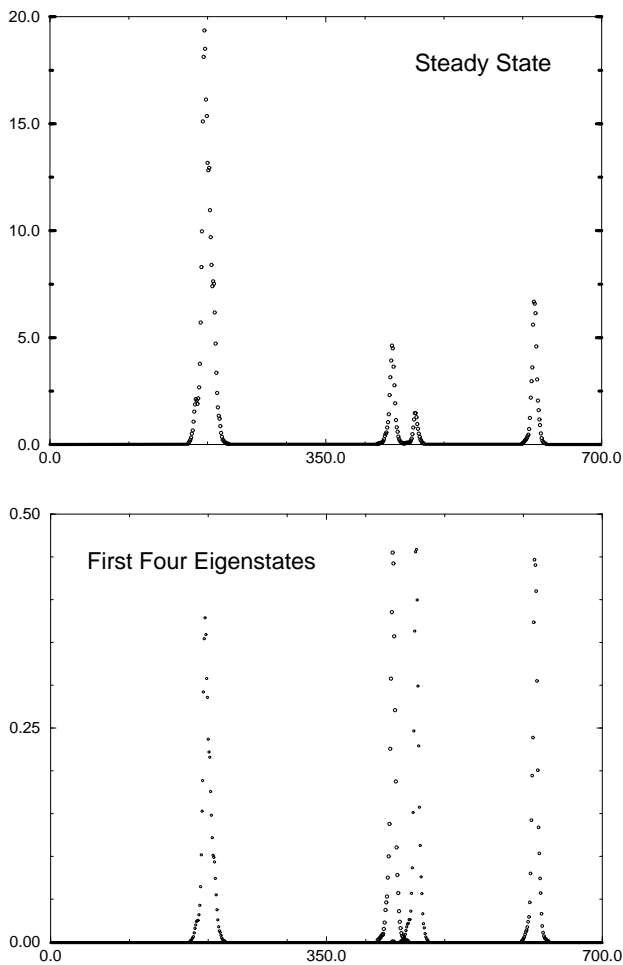


FIG. 6. (Top) Steady-state population distribution for a 700-site tight-binding model with site random growth rates and nonlinear interactions. (Bottom) Plots of the four unstable eigenfunctions obtained by linearizing the Liouville operator for the same realization of the random potential about the state of zero population. The positions of these eigenfunctions match perfectly the peaks in the steady state of the nonlinear problem. The heights of the peaks in the steady state are proportional to the *eigenvalues* of the corresponding eigenfunctions.

Fig. 6 with an accuracy of a few percent. Thus, a population of bacteria described by (1.2) or (1.18) evolves toward a steady-state distribution given by the ground state and first few excited states of a Schrödinger-like equation.

We next discuss the case shown schematically on the right side of Fig. 5, where a number of *delocalized* states have become unstable. This regime could be accessed either by increasing the mean growth rate a , or by increasing \mathbf{v} which enlarges the bubble of extended states. (To pin the center of the band one should actually increase v while holding $a - v^2/4D$ fixed). Because the Liouville operator is real, these delocalized modes occur in pairs: if $\phi_n^R(x)$ is a mode with eigenvalue Γ_n , then $\phi_n^R(x)^*$ is an eigenfunction with eigenvalue Γ_n^* . As shown

in detail by Brauwer *et al.* [30], these modes are (at least for weak randomness) approximately plane waves, characterized by nonzero wave vector pairs k and $-k$. The dynamics changes dramatically as soon as the first pair of delocalized eigenfunctions becomes relevant. Now, there will be nontrivial mode couplings between the newly unstable delocalized modes and each other, as well as with the unstable localized ones discussed earlier. By analogy with the physics of tilted vortex lines interacting with columnar defects [17,31], we now expect macroscopic occupation of modes near $q = 0$, similar to Bose-Einstein condensation. A broad background *extended* species population should now be superimposed on the peaks which represent localized modes, as indicated schematically in Fig. 7. The proportion of, say, bacteria incorporated into this background should increase with increasing a . Delocalization arises because populations can drift between growth “hot spots” instead of dying out when the convection velocity is high. According to the mode couplings in the Fourier basis displayed in Eq. (B.3) of Appendix B, fixed point value for the $q = 0$ mode is determined by the values of the unstable pairs $(k, -k)$.

There should be a large difference in the response of the steady state to a small change in \mathbf{v} for localized and delocalized steady states. The spectrum “unzips” further into the complex plane with increasing $v \propto g$ as more modes delocalize. For spectra like that on the left side of Fig. 5, these additional delocalized modes are irrelevant and should not affect the steady state. The only change occurs due to the distortion of the relevant localized modes according to Eq. (3.5). For spectra like those on the right side of Fig. 5, however, increasing \mathbf{v} (with $a - v^2/4D$ constant) leads to more *relevant* delocalized modes, with large changes in the corresponding steady state. Note that the “carrying capacity” defined by Eq. (3.11) *diverges* when $g \rightarrow \kappa_n$ and a mode described by an eigenfunction like (3.6) becomes delocalized. However, coupling coefficients such as (3.7) remain *finite* at the delocalization transition.

Although we have discussed the dynamics using one-dimensional spectra, we expect similar delocalization phenomena with increasing v or a with two-dimensional spectra such as that in Fig. 3b. If a is adjusted so that only a few localized modes are relevant, and the growth modes are strongly localized, the steady state should look like Fig. 4 with peak heights proportional to the growth eigenvalues. With increasing growth rate or convection velocity, eventually both delocalized *and* new localized modes should start to participate in the steady state. The coexistence of localized and extended eigenmodes at the same real part of the energy in $d = 2$ was discussed in [25]: anisotropic localized eigenfunctions for $\mathbf{g} = 0$ will delocalize sooner if their most extended direction coincides with the direction of \mathbf{g} . We expect that the resulting extended state wave functions are streaked out in the direction of \mathbf{g} , and that these streaks will be reflected into the steady-state species population.

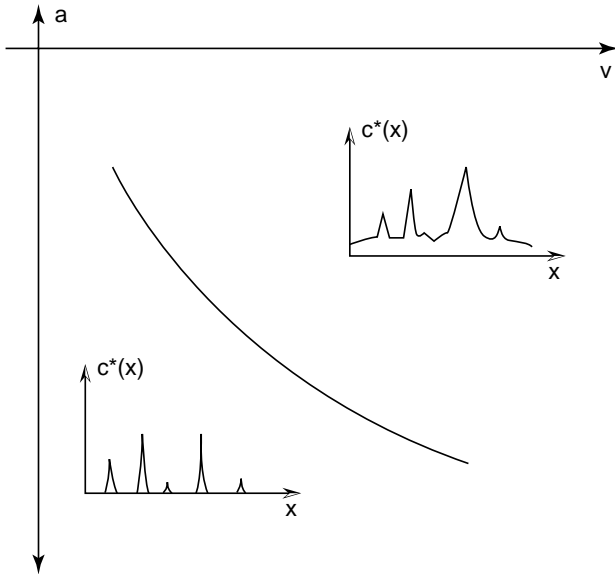


FIG. 7. Schematic “phase diagram” indicating regimes of localized steady states (lower left) and extended steady states (upper right) as a function of the average growth rate a and the convection velocity v . (A region of large negative a where all initial populations eventually become extinct is not shown.)

It is possible that a delocalization transition arises even for $\mathbf{v} = 0$ with increasing a (or increasing diffusion constant D). As the number or spatial extent of the relevant eigenmodes goes up, eventually the localized states begin to overlap. The steady state may become “extended” in this limit, in the sense that individual members of a species can hop easily from one growth hot spot to another. Again, the response of the steady state to a small change in convection velocity (away from zero) could be an indicator of this transition. A sharp transition is suggested by analogy with the “Bose glass” transition which occurs for increasing magnetic fields for vortices in Type II superconductors with columnar defects (see Appendix A and Ref. [17]).

A more detailed discussion of these interesting delocalization transitions will be presented in a future publication [32]. However, in the next two sections, we shall make some progress in describing the low-lying states which describe the growth modes in $d = 2$ for large convective velocities.

IV. BURGERS’ EQUATION AND THE LIMIT OF LARGE \mathbf{v}

A. Qualitative Discussion

We now study “unbounded growth” in the limit of large \mathbf{v} , with the goal of better understanding complicated spectra like those for the two-dimensional linearized growth problem shown in Fig. 3c. By large \mathbf{v}

we mean velocities so large that even the “ground state,” i.e., the growth mode with the largest eigenvalue, is delocalized,

$$v \gg D/\xi_0 \quad (4.1)$$

where ξ_0 is the localization length of the most rapidly growing eigenfunction. In this regime, it is helpful to exploit the analogy with the equilibrium statistical mechanics of a $2 + 1$ -dimensional vortex line described in Appendix A. In this analogy, a vortex trajectory represents the path taken by a particular growing population of, say, bacteria. As is evident from Fig. 10, when $v \rightarrow \infty$ the component of the “magnetic field” tilting the equivalent elastic vortex line leads to configurations more nearly perpendicular to the columnar defects representing the disordered growth rates. The transverse fluctuations of the tilted vortex line’s trajectory are unimpeded in the τ directions, while in the xy plane it sees the cross sections of the columnar defects. One might guess that in this large tilt limit the vortex simply wanders diffusively along the τ direction, but acts like a directed polymer in a $1 + 1$ -dimensional medium with point-like disorder when projected into the xy plane. More generally, the physics of tilted vortex lines with columnar pins in $d + 1$ dimensions should be related to directed polymers in $(d - 1) + 1$ dimensions with point-like disorder. A great deal is known about these problems [33].

To apply similar ideas to linearized population growth models, we assume that \mathbf{v} is in the x direction, and rewrite Eq. (1.16) as

$$\partial_t c + v \partial_x c = D \partial_x^2 c + D \nabla_{\perp}^2 c + [a + U(x, \mathbf{r}_{\perp})]c \quad (4.2)$$

where \mathbf{r}_{\perp} represents all spatial coordinates perpendicular to x . Specifically, we explore the long-time dynamics generated by this equation with a delta function initial condition,

$$\lim_{t \rightarrow 0} c(x, \mathbf{r}_{\perp}, t) = \delta(x) \delta^{d-1}(\mathbf{r}_{\perp}) \quad (4.3)$$

corresponding to a point inoculation of population at the origin. We look for a delocalized solution valid for long times in the limit of large v . The overall exponential time dependence generated by a , the constant part of the growth rate, and the diffusion with drift we expect in the (x, t) variables may be incorporated via the substitution

$$c(x, \mathbf{r}_{\perp}, t) = \frac{e^{at}}{\sqrt{4\pi Dt}} e^{\frac{-(x-vt)^2}{4Dt}} W(x, \mathbf{r}_{\perp}) \quad (4.4)$$

where $W(x, \mathbf{r}_{\perp})$ is to be determined. Note that $c(x, \mathbf{r}_{\perp}, t)$ becomes proportional to $\delta(x)$ as $t \rightarrow 0$, so the initial condition (4.3) requires

$$\lim_{x \rightarrow 0} W(x, \mathbf{r}_{\perp}) = \delta^{d-1}(\mathbf{r}_{\perp}). \quad (4.5)$$

Upon inserting Eq. (4.4) in (4.2), we find

$$\begin{aligned}
v\partial_x W(x, \mathbf{r}_\perp) + \frac{(x - vt)}{t} W(x, \mathbf{r}_\perp) \\
= D\partial_x^2 W(x, \mathbf{r}_\perp) + D\nabla_\perp^2 W(x, \mathbf{r}_\perp) \\
+ U(x, \mathbf{r}_\perp) W(x, \mathbf{r}_\perp). \quad (4.6)
\end{aligned}$$

According to the ansatz (4.4), $c(x, \mathbf{r}_\perp, t)$ is only appreciable for

$$|x - vt| \leq 2\sqrt{Dt} \quad (4.7)$$

so the second term on the left-hand side of (4.6) is smaller than the first by a factor of order $\sqrt{D/tv^2}$, and can be neglected in the limit of long times. In the remaining equation for $W(x, \mathbf{r}_\perp)$, which has no explicit time dependence, we expect that the term $\partial_x^2 W(x, \mathbf{r}_\perp)$ can be neglected for large x and t compared to the single x derivative which appears on the left-hand side. The resulting equation is an imaginary time Schrödinger equation, where x plays the role of “time”,

$$v\partial_x W(x, \mathbf{r}_\perp) \underset{t, x \rightarrow \infty}{\approx} D\nabla_\perp^2 W(x, \mathbf{r}_\perp) + U(x, \mathbf{r}_\perp) W(x, \mathbf{r}_\perp). \quad (4.8)$$

Note that the random “potential” $U(x, \mathbf{r}_\perp)$ depends both on the “time” x and on the additional $(d-1)$ spatial directions.

Consider the application of this mapping to two-dimensional species populations with strong convection. Assume for simplicity that $a > 0$, so that the population grows on average as it convects and diffuses downstream. For fixed x , the solution $W(x, y)$ of the resulting $(1+1)$ -dimensional Schrödinger equation (subject to the boundary condition (4.5)) describes the distribution in y of a growing species population which has traveled through random distribution of growth rates for a time of order $t = x/v$. The results of extensive studies of the Schrödinger equation in $1+1$ dimensions [33] with a space and time-dependent random potential may be interpreted as follows: For any fixed y value, imagine tracing the genealogy of, say, all bacteria which have reached particular position (x, y) . As $x \rightarrow \infty$, the *overwhelming majority* of bacteria near the point (x, y) will have evolved along a *spatially convoluted optimal path* of especially favorable growth rates. The fraction of bacteria whose ancestors come along this route is favored over all routes in $W(x, y)$ by an exponential factor $\sim \exp[c'x^\omega]$, where c' is a constant. The exponent ω (which describes the fluctuations in the ground state energy in the analogous problem in the statistical mechanics of flux lines) is known to be $\omega = 1/3$ exactly [33]. Any particular path $y(x)$ of optimal evolution itself wanders with typical transverse fluctuations which behave like

$$y(x) \sim x^\zeta \quad (4.9)$$

where $\zeta = \frac{\omega+1}{2} = 2/3$ is a universal critical exponent, independent of the exact probability distribution of the randomness and other details. *Because $2/3 > 1/2$, this*

optimal path will be well defined even in the presence of diffusion. A schematic of a set of optimal paths is shown in Fig. 8a. The population distribution $c(x, y, t = x/v)$ is sketched in Fig. 8b. The exponent ζ also controls the overall transverse spread in y of the spatially varying population for fixed x . This “superdiffusive” spreading ($\zeta > 1/2$) arises because trajectories which would be rare in conventional diffusion lead to strong amplification if they pass through regions of particularly favored growth. The exponent ω determines the *size* of the fluctuations in $c(x, y, t = x/v)$, which ride on top of an overall exponential growth, $c(x, y, t = x/v) \sim e^{ax/v}$.

Similar behavior is expected for the $2+1$ -dimensional random Schrödinger equation which results for convecting populations with randomness in $d = 3$, with the universal exponents $\zeta \approx 0.59 \approx 3/5$ and $\omega = 2\zeta - 1 = 1/5$ [33]. The growing population again becomes streaked-out in streamwise direction, but with a nontrivial wandering transverse to the stream.

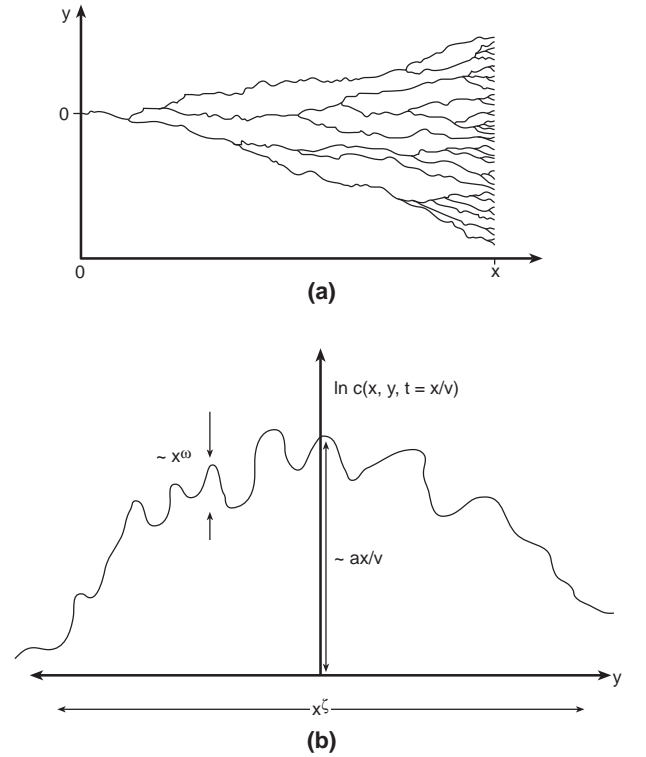


FIG. 8. (a) Trajectories for a growing species which will produce a particularly large population at the point (x, y) at time of order $t = x/v$. The population associated with a given point is spread over a region with typical size $\sqrt{Dx/v}$. For large x , bacteria which have traveled along such a path of favorable growth rates will dominate the population at (x, y) . (b) Schematic of the logarithm of the population $c(x, y, t = x/v)$ discussed above as a function of y . Typical fluctuations in population size away from simple exponential growth are of order $\exp[c'x^\omega]$, and the population from an initial source of point inoculation has spread out a distance of order x^ζ .

B. Average Growth Spectrum

We now study large v growth spectra like those in Figs. 2c and 3c averaged over many realizations of the disorder. Reference [25] presents numerical evidence and qualitative arguments that the effect of disorder on the spectrum of the non-Hermitian operator (1.13) in *one* dimension for large v is in fact very weak [34]. It was argued that the more complicated chaotic eigenvalue spectra observed in $d = 2$ were due to level repulsion of discrete eigenvalues in the complex plane. Here we first show explicitly that perturbation theory in the disorder simply leads to a “free particle” dispersion relation like Eq. (1.15) with renormalized values of a , v , and D in one dimension. We then demonstrate that the same perturbation analysis is singular in higher dimensions, consistent with the mapping onto a $(d - 1)$ -dimensional random Schrödinger equation described above.

For a given configuration of growth rates, we apply standard second-order perturbation theory [35] to the operator (1.13). The resulting growth rate spectrum, starting with a plane wave set of basis functions reads,

$$\epsilon(\mathbf{k}) = \epsilon_0(\mathbf{k}) + \langle \mathbf{k} | U | \mathbf{k} \rangle + \sum_{\mathbf{q}} \frac{|\langle \mathbf{q} | U | \mathbf{k} \rangle|^2}{\epsilon_0(\mathbf{k}) - \epsilon_0(\mathbf{q})} + O[U^3(\mathbf{x})] \quad (4.10)$$

where for a basis appropriate to the lattice growth model (1.20) with N sites, we have

$$|\mathbf{k}\rangle = \frac{1}{\sqrt{N}} \sum_{\mathbf{x}} e^{i\mathbf{k} \cdot \mathbf{x}} |\mathbf{x}\rangle, \quad (4.11)$$

and

$$\epsilon_0(\mathbf{k}) = a - i\mathbf{v} \cdot \mathbf{k} - Dk^2 + O(k^3), \quad (4.12)$$

with

$$\langle \mathbf{q} | U | \mathbf{k} \rangle = \frac{1}{N} \sum_{\mathbf{x}} e^{i(\mathbf{k} - \mathbf{q}) \cdot \mathbf{x}} U(\mathbf{x}). \quad (4.13)$$

The averages over disorder are easily calculated by first using this lattice model, and then passing to the continuum limit. With $U(\mathbf{x})$ uniformly distributed in the interval $[-\Delta, \Delta]$, we have

$$\overline{U(\mathbf{x})U(\mathbf{x}')} = \frac{1}{3}\Delta^2\delta_{\mathbf{x},\mathbf{x}'} \quad (4.14)$$

where the overbar represents a disorder average. It follows that

$$\overline{\langle \mathbf{k} | U | \mathbf{k} \rangle} = 0 \quad (4.15)$$

and

$$\overline{|\langle \mathbf{q} | U | \mathbf{k} \rangle|^2} = \Delta^2/3N. \quad (4.16)$$

With v in the x direction, we average over disorder and take the limit $N \rightarrow \infty$ in Eq. (4.10), and find

$$\begin{aligned} \bar{\epsilon}(k_x, k_\perp) &= \epsilon_0(k_x, k_\perp) + \frac{1}{3}l_0^d\Delta^2 \int \frac{dq_x}{2\pi} \\ &\times \int \frac{d^{d-1}q_\perp}{(2\pi)^{d-1}} \frac{1}{iv(q_x - k_x) + D(q^2 - k^2)} \end{aligned} \quad (4.17)$$

where l_0 is the lattice constant of a lattice and we have kept only the small k expansion displayed in Eq. (4.12).

Evaluation of the average spectrum is particularly simple in one dimension, because the transverse wave vectors \mathbf{k}_\perp and \mathbf{q}_\perp are absent. Upon extending the integration limits on q_x to $\pm\infty$, setting $q_x - k_x = p_x$ and symmetrizing in p_x , we have

$$\begin{aligned} \bar{\epsilon}(k_x) &= a - ivk_x - Dk_x^2 + \frac{1}{3}l_0\Delta^2 \\ &\times \int_{-\infty}^{\infty} \frac{dp_x}{2\pi} \frac{D}{D^2p_x^2 - (iv + 2Dk_x)^2} \\ &= a - ivk_x - Dk_x^2 + \frac{l_0\Delta^2 i}{6(iv + 2Dk_x)}. \end{aligned} \quad (4.18)$$

Expanding the disorder correction in k leads to renormalized values of a , v , and D

$$a_R = a + l_0\Delta^2/6v \quad (4.19a)$$

$$v_R = v - l_0\Delta^2 D/3v^2 \quad (4.19b)$$

$$D_R = D + 2l_0\Delta^2 D^2/3v^3 \quad (4.19c)$$

We see that disorder increases the mean growth rate, decreases the effective convective velocity, and increases the effective diffusion constant in an expansion in the dimensionless ratio $l_0\Delta^2 D/v^3$.

The new growth eigenfunctions are slightly perturbed plane waves [35]

$$|k\rangle' = |k\rangle + \sum_{q \neq k} \frac{\langle q | U | k \rangle}{\epsilon_0(k) - \epsilon_0(q)} |q\rangle \quad (4.20)$$

and are clearly still delocalized. Equation (4.19b) suggests that localization sets in whenever

$$\frac{l_0\Delta^2 D}{v^3} \geq 1, \quad (4.21)$$

i.e., localization occurs when the effective drift velocity is renormalized to zero. The physical basis for this criterion is as follows. In the absence of convection, the *maximum* growth rate associated with the operator (1.13) (i.e., the ground state eigenfunction of the corresponding Hamiltonian) will be given by minimizing the variational function

$$W[c(x)] = \frac{\int \left[\frac{D}{2} \left(\frac{dc(x)}{dx} \right)^2 - \frac{1}{2} U(x) c^2(x) \right] dx}{\int c^2(x) dx}. \quad (4.22)$$

The random potential $U(x)$ in the continuum limit now has correlator

$$\overline{U(x)U(x')} = \frac{1}{3} \Delta^2 l_0 \delta(x - x') \quad (4.23)$$

where l_0 is a microscopic cutoff, of order the lattice constant in a discrete growth model like (1.20). We assume an exponentially localized nodeless “ground state” growth eigenfunction centered on the origin $c_0(x) \sim \exp(-\kappa|x|)$, and replace the random part of (4.22) by its root-mean square value. Upon neglecting dimensionless coefficients of order unity, we find

$$W(\kappa) \sim D\kappa^2 - \Delta(l_0\kappa)^{1/2} \quad (4.24)$$

which is minimized for $\kappa = \kappa_0$, with

$$\kappa_0 \approx (\Delta l_0^{1/2}/D)^{2/3}, \quad (4.25)$$

and we again neglect constants of order unity. The “gauge transformation” (1.17) allows this state to remain localized only if $v/D \leq \kappa_0$, which is equivalent to the criterion (4.21).

We now demonstrate the singularities which arise for large $\mathbf{v}||\hat{\mathbf{x}}$ in higher dimensions $d \geq 2$. Upon setting

$$p_x = q_x - k_x, \quad \mathbf{p}_\perp = \mathbf{q}_\perp \quad (4.26)$$

and symmetrizing in p_x , Eq. (4.17) becomes

$$\begin{aligned} \bar{\epsilon}(k_x, \mathbf{k}_\perp) = & a - ivk_x - D_x k_x^2 - D_\perp k_\perp^2 \\ & + \frac{1}{3} \Delta^2 l_0^d \int \frac{dp_x}{2\pi} \int \frac{d^{d-1}p_\perp}{(2\pi)^{d-1}} \\ & \times \frac{D_x p_x^2 + D_\perp (p_\perp^2 - k_\perp^2)}{[D_x p_x^2 + D_\perp (p_\perp^2 - k_\perp^2)]^2 - p_x^2 (iv + 2D_x k_x)^2} \end{aligned} \quad (4.27)$$

where we have separated the diffusion term in $\epsilon_0(k_x, k_\perp)$ into components parallel and perpendicular to \mathbf{v} with $D_x = D_\perp = D$. It is tedious but straightforward to demonstrate that a , v , and D_x suffer only finite renormalizations similar to Eqs. (4.19) when this formula is expanded in k_x . However, upon setting $k_x = 0$ and we find a diverging renormalization of D_\perp in the long wavelength part of the integral,

$$D_\perp^R = D_\perp + \frac{\Delta^2 l_0^d}{12v} \int \frac{d^{d-1}p_\perp}{(2\pi)^{d-1}} \frac{1}{p_\perp^2} + \text{less singular terms.} \quad (4.28)$$

Consider the meaning of this infrared divergence for $d = 2$. In a finite system of spatial extent $L_y \ll L_x$ in the y direction, we have

$$D_\perp^R \approx D_\perp \left[1 + \alpha \frac{\Delta^2 l_0^2}{v D_\perp} L_y \right] \quad (4.29)$$

where α is a positive dimensionless coefficient. Thus a “free particle” spectrum of the form

$$\bar{\epsilon}_0(k_x, k_y) \approx a_R - iv_R k_x - D_x^R k_x^2 - D_\perp^R k_y^2 \quad (4.30)$$

is only a good approximation provided v is large enough such that

$$\frac{\Delta^2 l_0^2}{v D_\perp} L_y \leq 1. \quad (4.31)$$

Equation (4.31) is consistent with numerical results and a criterion based on a level repulsion argument for the lattice model [25]. However, for any fixed value of v , there will *always* be nontrivial changes in the growth spectrum for sufficiently large L_y , consistent with chaotic spectra like that exhibited in Fig. 3c. The mapping onto the physics of a $(d-1)$ -dimensional random Schrödinger equation suggests that, when evaluated to all orders in perturbation theory, the renormalized wave vector-dependent transverse diffusion constant actually diverges as $q_\perp \rightarrow 0$ [33], $D_\perp^R(q_\perp) \sim q_\perp^{1/\zeta-2}$, so that the disorder averaged renormalized spectrum takes the form, valid for small wave vectors,

$$\bar{\epsilon}(k_x, k_\perp) \approx a_R - iv_R k_x - D_x^R k_x^2 - A_\perp k_\perp^{1/\zeta}. \quad (4.32)$$

With $\zeta = 2/3$, we have

$$\bar{\epsilon}(k_x, k_y) \approx a_R - iv_R k_x - D_x^R k_x^2 - A_\perp k_y^{3/2} \quad (\text{two dimensions}). \quad (4.33)$$

This growth spectrum implies that length scales in the transverse direction scale with the $2/3$ power of stream-wise length scales, consistent with Eq. (4.9). The exponent $3/2$ controlling transverse fluctuations also appears in the renormalization group treatment of fluctuations in $\ln c(r, t)$ presented in Sec. 5. In $d = 3$, the mapping onto a random Schrödinger equation leads to an exponent $\zeta \approx 3/5$, and the small wave vector form,

$$\bar{\epsilon}(k_x, k_\perp) \approx a_R - iv_R k_x - D_x^R k_x^2 - A_\perp k_\perp^{5/3} \quad (\text{three dimensions}). \quad (4.34)$$

It is interesting to compute the consequences of spectra like (4.33) and (4.34) for a density of states in the complex plane, defined by

$$\begin{aligned} g(\epsilon_1, \epsilon_2) = & \int \frac{dk_x}{2\pi} \int \frac{d^{d-1}k_\perp}{(2\pi)^{d-1}} \delta[\epsilon_1 \\ & - \text{Re } \bar{\epsilon}(k_x, k_\perp)] \delta[\epsilon_2 - \text{Im } \bar{\epsilon}(k_x, k_\perp)]. \end{aligned} \quad (4.35)$$

Note that this is the density of states associated with disordered averaged *eigenvalues*. If the fluctuations of the eigenvalues away from their average values are small, this quantity will be the same as the disordered average *density of states* studied, e.g., in Ref. [22]. We measure

energies relative to a_R so that the top of the band (corresponding to the ground state of the equivalent Hamiltonian) occurs near the origin. Straightward calculations then lead to the predictions

$$\begin{aligned} g(\epsilon_1, \epsilon_2) &= 0, \quad \epsilon_1 > 0 \quad \text{or} \quad \epsilon_2^2 > -\epsilon_1 v_R^2 / D_x; \\ g(\epsilon_1, \epsilon_2) &\propto (|\epsilon_1| - D_x^R \epsilon_2^2 / v_R^2)^{-1/3}, \\ &\quad \text{otherwise (two dimensions)} \end{aligned} \quad (4.36)$$

and

$$\begin{aligned} g(\epsilon_1, \epsilon_2) &= 0, \quad \epsilon_1 > 0 \quad \text{or} \quad \epsilon_2^2 > -\epsilon_1 v_R^2 / D_x; \\ g(\epsilon_1, \epsilon_2) &\propto (|\epsilon_1| - D_x^R \epsilon_2^2 / v^2)^{1/5}, \\ &\quad \text{otherwise (three dimensions)} \end{aligned} \quad (4.37)$$

close to the band edge.

These results are valid for small real and imaginary energies ϵ_1 and ϵ_2 . The density of states thus vanishes outside a parabolic boundary, as in Fig. 3c and similar to its behavior in a pure system. However, it diverges as the boundary is approached in $d = 2$ and *vanishes* in $d = 3$ with new universal critical exponents when disorder is present. Disorder thus has a strong influence in the thermodynamic limit for large v when $d \geq 2$, even though all states are delocalized. In a *homogeneous* growth model, this density of states has a square root divergence near the boundary in $d = 2$ and approaches a constant in $d = 3$.

As a crude approximation, one could use the *average* growth spectrum to estimate the behavior of, for example $\bar{c}(x, y, t)$ in $d = 2$,

$$\bar{c}(x, y, t) \approx \int \frac{dk_x}{2\pi} \int \frac{dk_y}{2\pi} e^{\bar{\epsilon}(k_x, k_y)t} e^{ik_x x + ik_y y} c(k_x, k_y, t = 0) \quad (4.38)$$

where $c(k_x, k_y, t = 0)$ is the Fourier transformed initial condition. However, it is easier and more systematic to study the statistics of $\ln[c(x, t)]$, as is often case for systems with multiplicative noise. This is done in the next Section.

V. SPACE-TIME FLUCTUATIONS OF $\ln[c(\mathbf{x}, t)]$

In this section we give a detailed analysis of the response of a homogeneous biological system to the introduction of quenched random inhomogeneities in the growth rate. Let us look, for concreteness, at a *homogeneous* initial condition, i.e., $c(\mathbf{x}, t = 0) = \text{const.}$, which then evolves under the influence of some kind of quenched spatial randomness. As discussed in Section I, if the initial, constant density $c(\mathbf{x}, t = 0)$ is very small compared to a/b , the short time dynamics of this system is determined by Eq. (1.6), and for $c(\mathbf{x}, t) \approx c^*(\mathbf{x})$, i.e., near the stable fixed point, the long-time decay into c^* is given

by Eq. (1.8). The dynamic renormalization group approach presented here is thus directly relevant to the decay of small unstable fluctuations into the steady state or to the growth of unstable modes if b is small enough such that the long-time behavior of the linearized problem manifests itself before the nonlinear reaction term in (1.2) becomes important. Moreover, as discussed in Section III, the basic features of the linearized problem, such as its eigenvalues and eigenstates, can be used in certain limits to assess the nonlinear time evolution, as in Eq. (3.3).

We assume the term $-bc^2$ in (1.2) is negligible, and use the fact that $c(\mathbf{x}, t)$ is always nonnegative to define its logarithm $\Phi(\mathbf{x}, t)$, via the transformation

$$c(\mathbf{x}, t) = e^{\frac{\lambda}{2D} \Phi(\mathbf{x}, t) + at} c(\mathbf{x}, t = 0). \quad (5.1)$$

With $\mathbf{v} \parallel \hat{\mathbf{x}}$, the function $\Phi(\mathbf{x}, t)$ then satisfies (for a *uniform* initial species population)

$$\partial_t \Phi + v \partial_x \Phi = D \nabla^2 \Phi + \frac{\lambda}{2} (\nabla \Phi)^2 + U(\mathbf{x}), \quad (5.2)$$

with the initial condition $\Phi(\mathbf{x}, t = 0) = 0$. An identical equation was studied numerically and via a scaling ansatz by Chen *et al.* [21] as a model of charge density waves interacting with quenched disorder. Here, we use the renormalization group to study this problem analytically using the methods of Ref. [26].

We have singled out the direction parallel to the drift as x , while the $d - 1$ -dimensional perpendicular space will be denoted \mathbf{r}_\perp , as in Sec. 4. Equation (5.2) takes the form

$$\begin{aligned} \partial_t \Phi(\mathbf{r}_\perp, x, t) + v \partial_x \Phi(\mathbf{r}_\perp, x, t) = \\ D_\perp \nabla_\perp^2 \Phi(\mathbf{r}_\perp, x, t) + D_x \partial_x^2 \Phi(\mathbf{r}_\perp, x, t) \\ + \lambda_\perp (\nabla_\perp \Phi)^2 + \lambda_x (\partial_x \Phi)^2 + U(\mathbf{r}_\perp, x), \end{aligned} \quad (5.3)$$

with $D_\perp = D_x = D$, and $\lambda_\perp = \lambda_x = \lambda$. The random function $U(\mathbf{r}_\perp, x)$ satisfies

$$\overline{U(\mathbf{r}_\perp, x) U(\mathbf{r}'_\perp, x)} = \Upsilon \delta(x - x') \delta^{d-1}[\mathbf{r}_\perp - \mathbf{r}'_\perp] \quad (5.4)$$

where the correlator strength is related to the spread $[-\Delta, \Delta]$ of growth rates in a lattice model by $\Upsilon \propto \Delta^2 \ell_0^d$.

We now impose a change of scale

$$\mathbf{r}_\perp \rightarrow s \mathbf{r}_\perp \quad (5.5a)$$

$$x \rightarrow s^\eta x \quad (5.5b)$$

$$t \rightarrow s^z t \quad (5.5c)$$

$$\Phi \rightarrow s^\alpha \Phi \quad (5.5d)$$

where s is a renormalization group scale factor.

Under this scale transformation the parameters of Eq. (5.3) change according to

$$D_\perp \rightarrow s^{z-2} D_\perp$$

$$D_x \rightarrow s^{z-2\eta} D_x$$

$$\begin{aligned}
\Upsilon &\rightarrow s^{2z-2\alpha-(d-1)-\eta}\Upsilon \\
\lambda_\perp &\rightarrow s^{z+\alpha-2}\lambda_\perp \\
\lambda_x &\rightarrow s^{z+\alpha-2\eta}\lambda_\perp \\
v &\rightarrow s^{z-\eta}v
\end{aligned} \tag{5.6}$$

If the nonlinearities are absent, i.e., $\lambda_x = \lambda_\perp = 0$, Eq. (5.3) becomes exactly solvable. In this case, $\Phi(\mathbf{r}_\perp, x, t)$ is given by

$$\begin{aligned}
\Phi(\mathbf{r}_\perp, x, t) &= \int_{-\infty}^{\infty} \frac{d\omega}{2\pi} \int_{-\infty}^{\infty} \frac{dk_x}{2\pi} \\
&\times \int \frac{d^{d-1}k_\perp}{(2\pi)^{d-1}} \Phi(k_\perp, k_x, \omega) e^{i\mathbf{k}_\perp \cdot \mathbf{r}_\perp} e^{ik_x x} e^{-i\omega t}
\end{aligned} \tag{5.7}$$

where the Fourier transform of $\Phi(\mathbf{r}_\perp, x, t)$, satisfies

$$\Phi(\mathbf{k}_\perp, k_x, \omega) = G_0(\mathbf{k}_\perp, k_x, \omega) U(\mathbf{k}_\perp, k_x, \omega) \tag{5.8}$$

Note that since the disorder is time independent, its Fourier transform satisfies

$$U(\mathbf{q}_\perp, q_x, \omega) = \tilde{U}(\mathbf{q}, q_x) 2\pi \delta(\omega),$$

and

$$\langle \tilde{U}(\mathbf{k}, k_x) \tilde{U}(\mathbf{k}', k'_x) \rangle = \Upsilon (2\pi)^d \delta(\mathbf{k}_\perp - \mathbf{k}'_\perp) \delta(k_x - k'_x). \tag{5.9}$$

The bare propagator $G_0(\mathbf{k}_\perp, k_x, \omega)$ is

$$G_0(\mathbf{k}_\perp, k_x, \omega) = \frac{1}{-i\omega + ivk_x + D_x k_x^2 + D_\perp k_\perp^2}. \tag{5.10}$$

In this case the naive scaling treatment gives exact results. From Eqs. (5.6) one finds that keeping D_\perp , Δ and v fixed under the scale transformation requires

$$z = 2, \quad \eta = 2, \quad \alpha = \frac{3-d}{2}. \tag{5.11}$$

The term proportional to D_x then scales to zero, confirming that it is negligible at long wavelengths and low frequencies compared to the single derivative in the convective term. The same analysis suggests that the nonlinear coupling λ_x is also irrelevant, $\lambda_x \rightarrow s^{-(1+d)/2}\lambda_x$, while $\lambda_\perp \rightarrow s^{3-d/2}\lambda_\perp$ so that $d = 3$ is the upper critical dimension for this problem.

These results become easier to understand if we consider their impact on a concrete physical quantity. Following Ref. [21], we consider the sample-to-sample fluctuations in $\Phi(\mathbf{r}_\perp, x, t)$ in different random environments all with the same physical dimensions L_x and L_\perp ,

$$\begin{aligned}
W(L_x, L_\perp) &= \overline{\Phi^2(x, \mathbf{r}_\perp, t)} \\
&= \ln^2[c(x, \mathbf{r}_\perp, t)e^{-at}].
\end{aligned} \tag{5.12a}$$

For population dynamics of, say, bacteria, one could divide a single large colony into many patches with these

dimensions to calculate the average. It is straightforward to show that the simple scaling of the linear theory sketched above implies that $W(L_x, L_\perp)$ takes the form, for $d = 2$

$$W(L_x, L_\perp) = L_x^\chi h(L_\perp/L_x^\zeta) \tag{5.12b}$$

where $\chi = 1/2$ and $\zeta = 1/2$. To obtain (5.12b), use Eq. (5.23) below with the Gaussian exponents from (5.11). The same results follow directly from Eq. (5.8) [21]

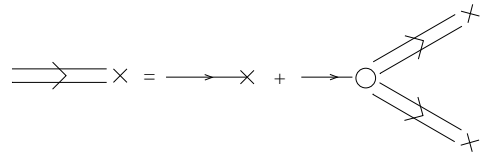
$$W(L_x, L_\perp) = \int_{q_x < L_x^{-1}} \frac{dq_x}{2\pi} \int_{q_\perp < L_\perp^{-1}} \frac{dq_\perp}{(2\pi)} \frac{\Upsilon}{v^2 q_x^2 + D_\perp^2 q_\perp^4} \tag{5.12c}$$

which also leads to the conclusion that $h(x) \sim x$ for large x . Chen *et al.* simulated the full nonlinear equation (5.2) in $d = 2$ and found $\chi = 0.5 \pm 0.05$ and $\zeta = 0.85 \pm 0.05$. Below we determine these exponents exactly.

To consider systematically the effect of the nonlinearities, we perform a perturbative expansion around the exact solution embodied in (5.7–5.10) in powers of λ_\perp and λ_x . We begin by rewriting (5.7) as an integral over the momentum up to some cutoff:

$$\begin{aligned}
\Phi(\mathbf{r}_\perp, x, t) &= \int_{-\infty}^{\infty} \frac{d\omega}{2\pi} \int_{-\infty}^{\infty} \frac{dk_x}{2\pi} \int_0^\Lambda \frac{d^{d-1}k_\perp}{(2\pi)^{d-1}} \\
&\times \Phi(\mathbf{k}_\perp, k_x, \omega) e^{i\mathbf{k}_\perp \cdot \mathbf{r}_\perp} e^{ik_x x} e^{-i\omega t}
\end{aligned} \tag{5.13}$$

(a)



(b)

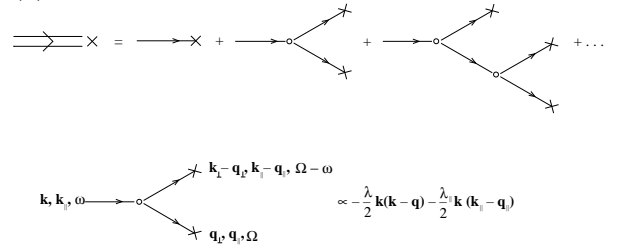


FIG. 9. (a) Diagrammatic representation of the integral equation (5.14). (b) Iteration solution of Eq. (5.14) and this meaning of the vertex in this diagrammatic series.

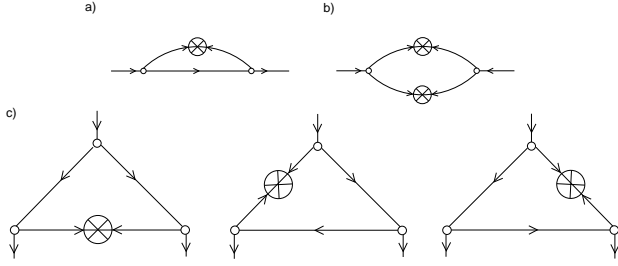


FIG. 10. (a) One-loop correction to the self-energy obtained by averaging over the noise. (b) Perturbative correction to the two-point function $\Phi(\mathbf{x}, t)\Phi(\mathbf{0}, 0)$. (c) Three diagrams which contribute to the one-loop effective vertex renormalization.

Here, Λ is a cutoff initially of order ℓ_0^{-1} , where ℓ_0 is a microscopic length scale of order the lattice constant. Equation (5.3) now becomes

$$\begin{aligned} \Phi(\mathbf{k}_\perp, k_x, \omega) = G_0(\mathbf{k}_\perp, k_x, \omega) & \left[U(\mathbf{q}_\perp, q_x, \omega) + \int_{-\infty}^{\infty} \frac{d\Omega}{2\pi} \right. \\ & \int_{-\infty}^{\infty} \frac{dq_x}{2\pi} \int_0^\Lambda \frac{d^{d-1}\mathbf{q}_\perp}{(2\pi)^{d-1}} \\ & \left(-\frac{\lambda_\perp}{2} \mathbf{q}_\perp \cdot [\mathbf{k}_\perp - \mathbf{q}_\perp]_\perp - \frac{\lambda_x}{2} q_x [k_x - q_x] \right) \\ & \left. \Phi(\mathbf{k}_\perp - \mathbf{q}_\perp, k_x - q_x, \omega - \Omega) \Phi(\mathbf{q}_\perp, q_x, \Omega) \right] \end{aligned} \quad (5.14)$$

which can be represented graphically as in Fig. 9a. The formal iterative solution of (5.14) is shown in Fig. 9b.

The self-energy $\Sigma(\mathbf{k}_\perp, k_x, \omega)$ (Fig. 10a) yields the renormalized velocity v_R and diffusion constants D_\perp^R and D_x^R . The renormalization of Υ is represented by the graph in Fig. 10b, and vertex renormalization graphs for λ_x and λ_\perp are shown in Fig. 10c. The corrections to λ_\perp , λ_x , D_x and v do not diverge in the infrared limit in any dimension; naive perturbation theory yields, however, infrared divergent corrections to D and Υ for $d \leq 3$ as one takes the limit $\mathbf{k} \rightarrow 0$,

$$\delta D = K_{d-1} \left(\frac{\lambda^2 \Upsilon}{2D^2|v|} \right) \left(\frac{3-d}{4d-4} \right) \int_0^\Lambda dq q^{d-4} \quad (5.15)$$

$$\delta \Upsilon = K_{d-1} \left(\frac{\lambda^2 \Upsilon}{8D^2|v|} \right) \int_0^\Lambda dq q^{d-4} \quad (5.16)$$

where $K_d = S_d/(2\pi)^d$ and S_d is the surface area of the d -dimensional unit sphere. Equation (5.15) is similar to the result (4.28) obtained by considering the average growth rate. Equations (5.15) and (5.16) confirm that the upper critical dimension of theory is $d = 3$, below which renormalization group techniques are needed to take care for the infrared divergences of the loop integrals. Upon carrying out the procedure of Ref. [26], we find that the renormalization group flow equations for the relevant variables take the form

$$\frac{dD_\perp}{dl} = D_\perp \left[z - 2 + K_{d-1} \left(\frac{3-d}{4d-4} \right) g^2 \right] \quad (5.17)$$

$$\frac{d\Delta}{dl} = \Delta \left[2z - d + 1 - 2\alpha - \eta + K_{d-1} \frac{g^2}{4} \right] \quad (5.18)$$

$$\frac{d\lambda_\perp}{dl} = \lambda_\perp [\alpha + z - 2] \quad (5.19)$$

$$\frac{dv}{dl} = v [z - \eta] \quad (5.20)$$

We have set $s \equiv e^{-\ell}$, reduced the cutoff from Λ to $e^{-\ell}\Lambda$, and the corrections to the naive scaling results (5.6) are proportional to the dimensionless coupling constant,

$$g^2 \equiv \frac{\Delta \lambda^2}{2D^3|v|}. \quad (5.21)$$

The couplings D_x and λ_x again scale to zero, even at the nontrivial fixed point discussed below.

We now set $\eta = z$ and $\alpha = 2 - z$ to ensure that λ_\perp and v remain unchanged by our renormalization procedure. Using Eqs. (5.17)–(5.20) we can calculate the flow of the coupling constant g ,

$$\frac{dg}{dl} = \frac{3-d}{2} g + K_d \left(\frac{2d-5}{4d-4} \right) g^3. \quad (5.22)$$

The fixed point g^* is obtained by taking $\frac{dg}{dl} = 0$. For $d = 2$ (i.e., two-dimensional disordered growth model with one parallel and one perpendicular direction) the Gaussian fixed point at $g^* = 0$ is unstable, while $g^* = \left(\frac{2}{K_{d-1}} \right)$ is an attractive fixed point which corresponds to $\alpha = 1/2$, $z = 3/2$, and $\eta = 3/2$ (η should be equal to z since there are no infrared diverging correction to v).

We now integrate the recursion relations until ℓ is large, so that all transients have died off. The renormalization group homogeneity relation for the mean square fluctuations in $\ln[x(z, \mathbf{r}_\perp, t)e^{-at}]$ in a system with dimension L_x and L_\perp then reads

$$W(L_x, L_\perp) = e^{4\ell - 2z\ell} W(L_x e^{-z\ell}, L_\perp e^{-\ell}) \quad (5.23)$$

The prefactor follows from Eq. (5.5d), with $\eta = z$ and $\alpha = 2 - z$; we expect these results to be correct to all orders in perturbation theory due to the Galilean invariance of the problem after averaging over disorder [33]. Upon choosing $\ell = \ell^*$ such that $L_x e^{-z\ell^*} = 1$, Eq. (5.23) can be rewritten in a scaling form similar to (5.12b),

$$W(L_x, L_y) = L_x^{4\zeta - 2} h(L_\perp/L_x^\zeta) \quad (5.24)$$

where

$$\zeta = 1/z. \quad (5.25)$$

We have thus confirmed the scaling ansatz Eq. (5.5b) [21] with the specific predictions $\eta = 1/z = 2/3$ and $\chi = 4\zeta - 2 = 2/3$. These exact exponents differ somewhat, however, from the numerical estimates of Chen *et*

al. [21]; it would be interesting to see if the agreement improves with larger system sizes.

For $d = 3$, there is no perturbatively accessible fixed point of the one loop recursion relation (5.22). However, extensive numerical work exists suggesting a stable non-trivial fixed point with $z \approx 5/3$. Thus we predict from Eq. (5.23) that the scaling relation (5.5b) holds, with $\zeta = 1/z = 3/5$ and $\chi = 4\zeta - 2 = 2/5$ in $d = 3$.

Our analysis of the evolution of $\ln[c(\mathbf{x}, t)]$ shows in effect that the asymptotic behavior of the nonlinear equation (5.2) has the same critical exponents as a conventional noisy Burgers equation [23] with one less dimension. The same dimensional reduction for critical exponents $d \rightarrow (d-1)$ was described for the original linearized growth model in Sec. IVa. A related dimensional reduction has been found by Tang *et al.* [36] for a model of driven depinning in anisotropic media, and by Obukhov for directed percolation [37].

It is interesting to comment about the role of v in this perturbative renormalization calculation. The small dimensionless parameter of the series, g , is proportional to $1/v$ and diverges as $v \rightarrow 0$. When $v \rightarrow 0$ the theory is in the strong coupling limit where we expect *localized* states in the band tail. A signal of this phase transition is the (finite) one loop correction to v obtained from Eq. (5.14)

$$\delta v \propto -v \int \frac{dq q^{d-2}}{(4D_x D_\perp q^2 + v^2)^{3/2}}. \quad (5.26)$$

Although this correction is finite it suggests the existence of a critical value of v below which v_R is zero, consistent with localized states unaffected by convection.

ACKNOWLEDGMENTS

It is a pleasure to acknowledge helpful conversations with H. Berg, E. Budrene, K. Dahmen, D. Fisher, B.I. Halperin, T. Hwa, M. Kardar, A. Lesniewski and J. Pelletier. We thank N. Hatano for conversations and generous help with the figures. Finally, we are indebted to P. Grassberger for comments and for bringing Refs. [18–20] to our attention. This research was supported by the National Science Foundation through Grant No. DMR94–17047, and by the Harvard Materials Research Science and Engineering Laboratory through Grant No. DMR94–00396. One of us (N.S.) acknowledges the support of Bar-Ilan University and a Rothschild Fellowship.

APPENDIX A: POPULATION DYNAMICS AND VORTEX CONFIGURATIONS

In this appendix we review the statistical mechanics of a superconducting vortex line with a columnar pinning potential [17], and show that its partition function evolves with sample thickness in the same way as the linearized population dynamics problem studied here. The

different configurations of the vortex line, described here simply as an elastic string, are related to possible space-time trajectories of populations which diffuse, grow and drift in an inhomogeneous but time-independent environment.

Consider a superconductor sample of thickness L , pierced by “columnar pins,” which are long aligned columns of damaged material, illustrated schematically in Fig. 11. The vortex can usually be described by a single valued trajectory $\mathbf{r}(\tau)$, where we assume defects are aligned with the τ direction, $\tau = \mathbf{x} \times \mathbf{y}$. The free energy of this problem may be written as:

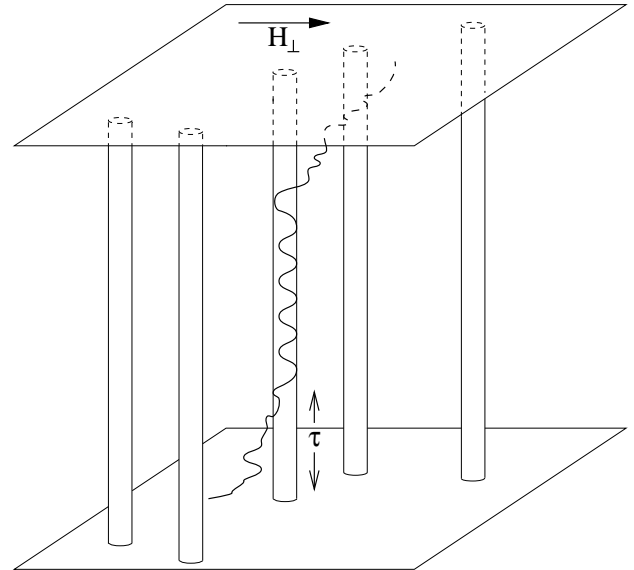


FIG. 11. Vortex line in a superconductor with columnar disorder. If $H_\perp = 0$, the flux line is localized, i.e., trapped by one or few pins into some region in the plane perpendicular to the correlated disorder. The coordinate τ along the columns plays role of time. As the external magnetic field is tilted away from the columns, the flux line tends to delocalize and tilt in the direction of the external field.

$$F[\mathbf{r}(\tau)] = \frac{\epsilon}{2} \int_0^L d\tau \left(\frac{d\mathbf{r}(\tau)}{d\tau} \right)^2 + \frac{1}{2} \int_0^L d\tau V[\mathbf{r}(\tau)] - \mathbf{H}_\perp \frac{\phi_0}{4\pi} \int_0^L d\tau \left(\frac{d\mathbf{r}}{dz} \right) \quad (A.1)$$

where ϵ is the tilt modulus of the flux line and the elastic contribution $\frac{\epsilon}{2} \left(\frac{d\mathbf{r}(\tau)}{d\tau} \right)^2$ is the first nontrivial term in the small tipping angle expansion of the line energy of a nearly straight vortex line. $V(\mathbf{r})$ is the random potential which arises from a τ -independent set of disorder-induced columnar pinning potentials (with its average value subtracted off), and \mathbf{H}_\perp is a perpendicular magnetic field.

The partition function $\mathcal{Z}(\mathbf{x}, \tau; \mathbf{x}_0, 0)$ associated with a vortex which start at position \mathbf{x}_0 at the bottom of the

sample ($\tau \equiv 0$) and terminates at position \mathbf{x} at temperature T somewhere in the interior at height τ is given by a path integral:

$$\mathcal{Z}(\mathbf{x}, \tau; \mathbf{x}_0, 0) = \int_{\mathbf{r}(0)=\mathbf{x}_0}^{\mathbf{r}(\tau)=\mathbf{x}} \mathcal{D}\mathbf{r}(\tau) \left[-\mathcal{F}[\mathbf{r}(\tau)]/T \right] \quad (\text{A.2})$$

Standard path integral techniques [16] may be used to show that $\mathcal{Z}(\mathbf{x}, \tau; \mathbf{x}_0, 0)$ obeys the Schrödinger-like equation,

$$-T \frac{\partial \mathcal{Z}}{\partial \tau} = -\frac{T^2}{2\epsilon} \nabla^2 \mathcal{Z} - \frac{T}{\epsilon} \mathbf{h}_\perp \cdot \nabla \mathcal{Z} + \frac{h_\perp^2}{2\epsilon} \mathcal{Z} + V(\mathbf{x}) \mathcal{Z} \quad (\text{A.3})$$

where $\mathbf{h}_\perp \equiv \frac{\mathbf{H}_\perp \phi_0}{4\pi}$ is the dimensionless perpendicular field. Thus, the growth of the partition function $\mathcal{Z}(\mathbf{x}, \tau)$ of a flexible line with height τ is the same as linearized population growth model Eq. (1.6), with the identifications $\tau \rightarrow t$, $D \rightarrow T/\epsilon$, $\mathbf{v} \rightarrow \mathbf{h}_\perp/\epsilon$, $U(\mathbf{x}) \rightarrow V(\mathbf{x})/T$ and $a \rightarrow h_\perp^2/2\epsilon T$.

Because

$$\lim_{\tau \rightarrow 0} \mathcal{Z}(\mathbf{x}, \tau; \mathbf{x}_0, 0) = \delta^d(\mathbf{x} - \mathbf{x}_0) \quad (\text{A.4})$$

the full partition function $\mathcal{Z}(\mathbf{x}, \tau; \mathbf{x}_0, 0)$ is in fact the Green's function for Eq. (1.6), assuming a delta function initial condition of population at position \mathbf{x}_0 and time $t = \tau = 0$.

APPENDIX B: MEAN FIELD THEORY OF HOMOGENEOUS POPULATION DYNAMICS

We start with the homogeneous analogue of Eq. (1.2),

$$\frac{\partial}{\partial t} c(\mathbf{x}, t) + \mathbf{v} \cdot \nabla c(\mathbf{x}, t) = D \nabla^2 c(\mathbf{x}, t) + ac(\mathbf{x}, t) - bc^2(\mathbf{x}, t) \quad (\text{B.1})$$

Upon decomposing $c(\mathbf{x}, t)$ into Fourier modes

$$c(\mathbf{x}, t) = \frac{1}{\Omega} \sum_{\mathbf{k}} c_{\mathbf{k}}(t) e^{i\mathbf{k} \cdot \mathbf{x}} \quad (\text{B.2})$$

where Ω is the volume of a d -dimensional box with periodic boundary conditions, we have

$$\frac{dc_{\mathbf{k}}(t)}{dt} = \Gamma_{\mathbf{k}} c_{\mathbf{k}} - \frac{b}{\Omega} \sum_{\mathbf{q}, \mathbf{q}'} c_{\mathbf{q}}(t) c_{\mathbf{q}'}(t) \delta_{\mathbf{k}, \mathbf{q}+\mathbf{q}'} \quad (\text{B.3})$$

with the complex growth spectrum

$$\Gamma_{\mathbf{k}} = a + i\mathbf{v} \cdot \mathbf{k} - Dk^2. \quad (\text{B.4})$$

In the spirit of Bogoliubov approximation for the collective excitations in superfluids [36], we separate out the $\mathbf{k} = 0$ mode and write

$$\frac{dc_0(t)}{dt} = ac_0 - \frac{b}{\Omega} c_0^2 - \left[\frac{b}{\Omega} \sum_{\mathbf{q} \neq 0} c_{\mathbf{q}}(t) c_{\mathbf{k}-\mathbf{q}}(t) \right] \quad (\text{B.5})$$

$$\frac{dc_{\mathbf{k}}(t)}{dt} = \Gamma_{\mathbf{k}} c_{\mathbf{k}} - \frac{2b}{\Omega} c_0(t) c_{\mathbf{k}}(t) - \left[\frac{b}{\Omega} \sum_{\mathbf{q} \neq 0, \mathbf{q}' \neq \mathbf{k}} c_{\mathbf{q}}(t) c_{\mathbf{k}-\mathbf{q}'}(t) \right] \quad (\text{B.6})$$

The mean field approximation consists of neglecting terms in the modes with $\mathbf{k} \neq 0$, shown in brackets in Eqs. (B.5) and (B.6). The approximate differential equations which remain have solutions

$$c_0(t) = \frac{\Omega \bar{c}_0 e^{at}}{[1 + \frac{b\bar{c}_0}{a}(e^{at} - 1)]} \quad (\text{B.7})$$

$$c_{\mathbf{k}}(t) = \frac{c_{\mathbf{k}}(0) e^{\Gamma_{\mathbf{k}} t}}{[1 + \frac{b\bar{c}_0}{a}(e^{at} - 1)]^2} \quad (\text{B.8})$$

where $\bar{c}_0 = \Omega c_0(t=0)$. The time evolution of $c(\mathbf{x}, t)$ is now completely determined by inserting these results into Eq. (B.2). Note that there are many growing modes with $\mathbf{k} \neq 0$ at short times when $a > 0$. However, when $t \gg \ln(b\bar{c}_0/a)$ the denominators of Eqs. (B.7) and (B.8) cause $c_0(t)$ to approach $c_0 = a/b$, and all modes with $\mathbf{k} \neq 0$ to decay away with the spectrum (1.16).

APPENDIX C: DENSITY OF STATES NEAR THE BAND EDGE

In this appendix we calculate the density of states (DOS) in the tail of the band of growth rates, i.e., near the ground state. We set the growth bias $a \equiv 0$, since it does not affect the statistics of the DOS. The discussion below assumes localized eigenmodes in the “relevant” or unstable part of the spectrum, where the convection term $\mathbf{g} \propto \mathbf{v}$ just produces a trivial shift in the eigenvalues, and hence we neglect \mathbf{g} as well.

Consider, then, a d -dimensional hypercubic lattice with edge length ℓ_0 , where the potential energy at each site is in the range $U(\mathbf{x}) \in [-\Delta, \Delta]$. Unbounded probability measures may give different results.

The continuum Liouville operator approximated by the lattice model may be written as:

$$\mathcal{L} = D\nabla^2 + U(\mathbf{x}). \quad (\text{C.1})$$

It is easy to see that the DOS function $\rho(E)$ in this model is bounded from above by Δ , such that $\rho(E) \rightarrow 0$ as $E \rightarrow \Delta$. The tail of the DOS is determined by the range of energies in which the DOS is determined by rare events, characterized by large spatial regions with low potential energy [38].

Let us estimate these fluctuations in the following way: the probability to find a hypersphere of radius R which contains only blocks of potential energy U larger than $\Delta - V_0$ is approximately

$$P(R, U > \Delta - V_0) \approx \left(\frac{V_0}{2\Delta}\right)^{(R/\ell_0)^d} \approx \exp\left[\left(\frac{R}{\ell_0}\right)^d \ln\left(\frac{V_0}{2\Delta}\right)\right]. \quad (\text{C.2})$$

The energy of a state confined by this rare fluctuation is given approximately by

$$E \approx \Delta - V_0 - D/R^2, \quad (\text{C.3})$$

so that the probability to get an energy between E and $E + dE$ using a sphere of radius R is $p(R, E) \sim \frac{\partial P}{\partial V_0}|_{V_0=E}$, i.e.,

$$p(R, E) \sim \exp\left[\left(\frac{R}{\ell_0}\right)^d \ln\left(\frac{1}{2} - \frac{E}{2\Delta} - \frac{D}{2R^2\Delta}\right)\right]. \quad (\text{C.4})$$

This expression is well defined for $\sqrt{\frac{D}{\Delta-E}} \leq R < \infty$. Optimizing $p(R, E)$ with respect to R gives, up to logarithmic corrections, a maximum at the lower limit $R^* \approx \sqrt{D/(\Delta-E)}$, so that as $E \rightarrow \Delta$ from below, $p(E) \equiv p(R^*, E)$ vanishes according to

$$p(E) \sim \exp[-(D/\ell_0^2[\Delta-E])^{d/2}]. \quad (\text{C.5})$$

Now the DOS is proportional to $p(E)$, i.e., at the tail of the distribution we have $g(E) \sim g_0 p(E)$, where g_0 is some normalization of order the DOS in the middle of the band.

Let us consider now the tight-binding analog of the above model. The on site potential is $U(\mathbf{x})$, taken from a square distribution in the range $[-\Delta, \Delta]$. The Liouvillian is, from Eq. (1.20),

$$\tilde{\mathcal{L}} = \frac{w}{2} \sum_{\mathbf{x}} \sum_{\nu=1}^d [|\mathbf{x}\rangle\langle\mathbf{x} + \mathbf{e}_\nu| + |\mathbf{x} + \mathbf{e}_\nu\rangle\langle\mathbf{x}|] + \sum_{\mathbf{x}} U(\mathbf{x}) |\mathbf{x}\rangle\langle\mathbf{x}|. \quad (\text{C.6})$$

The eigenenergies of this Hamiltonian are bounded, $-\Delta - w < \epsilon_n < \Delta + w$ with $w \sim D/\ell_0^2$. The states in the tails correspond to rare spatial fluctuations of $U(\mathbf{x})$. The probability to find such fluctuations (e.g., a region of radius R in which the on site potential is within a specified energy interval V_0 of the maximum value Δ) is the same as in the previous model. The energy spectrum of such fluctuation is given approximately by

$$\epsilon = \Delta - V_0 + w \sum_{\nu=1}^d \cos(k_\nu \ell_0), \quad (\text{C.7})$$

where $k \approx k_{\min} \sim 1/R$. Thus, states in this tail obey the relation

$$\epsilon \sim \Delta + w - V_0 - w/R^2 \quad (\text{C.8})$$

so that a result of the form (C.5) is applicable here also, with the energy measured from the edge of the band defined by the lattice model [39].

We can use the density of states result (C.5) and the eigenvalue spectra displayed in Figs. 2 to understand the results of Refs. [19] and [20] for particles diffusing and drifting with random traps in one dimension. We start with the expansion of $c(\mathbf{x}, t)$ in the complete set of eigenfunctions of Eq. (1.2) with $b = 0$, as in Eq. (2.1). For $\mathbf{v} = \mathbf{g} = 0$, all eigenvalues Γ_n are real and negative for this problem. As discussed in [20], the eigenvalues close to zero arise from the rare regions discussed above for the density of states. The spectrum for the lattice model will look like Fig. (2a), with however the top of the band just touching the origin. Upon assuming a uniform initial condition $c(\mathbf{x}, 0)$, we take all $c_n \sim \text{const}$ and integrate over space to obtain

$$N_{tot} = \int d^d \mathbf{x} c(\mathbf{x}, t) \propto \int_{-\infty}^0 g(\Gamma) e^{\Gamma t} d\Gamma \quad (\text{C.9})$$

Where $g(\Gamma)$ is the density of states. At $t \rightarrow \infty$, the behavior of the total number of surviving particles is dominated by energies near the top of the band, where

$$g(\Gamma) \propto \exp[-|\Gamma_0/\Gamma|^{d/2}]. \quad (\text{C.10})$$

A saddle point evaluation of Eq. (C.9) in d dimensions then leads to

$$N_{tot}(t) \propto \exp[-(t/t_0)^{\frac{d}{d+2}}], \quad (\text{C.11})$$

in agreement with Refs. [19] and [20].

For $v = g < g_1$, the effect of nonzero convection is simply a rigid downward shift of the spectrum, by an amount of $v^2/4D$ [20]. When $g > g_1$ in one dimension, the bubble of delocalized states shown in fig. (2b) will appear in the center of the band of negative eigenvalues. However, the behavior of the density of states at the top of band is unchanged, and we find

$$N_{tot}(t) \propto \exp[-\frac{v^2 t}{4D}] \exp[-(t/t_0)^{1/3}] \quad (\text{C.12})$$

in agreement with Ref. [19]. Delocalization affects the long time decay only when $g > g_2$, when *all* states are delocalized, as in Fig. 2c. The density of states in one dimension is then

$$g(\Delta\Gamma) \propto 1/(\Delta\Gamma)^{1/2} \quad (\text{C.13})$$

which leads an additional exponential contribution to the decay of Eq. (C.9) (up to logarithmic corrections), in qualitative agreement with the transition as a function of the bias found by Movaghar et. al. [19]. It would be

interesting to use the spectra displayed in Figs. 2 and 3 to extract the short and intermediate time behavior of N_{tot} , as well as the effect of drift in higher dimensions.

Note that the delocalization transition which describes particles diffusing and convecting in the presence of traps occurs at the *top* of the band. For population biology problems, one must consider *positive* growth eigenvalues and the phenomena of interest typically occur for $g_1 < g < g_2$. The localization transition of interest to us in this paper occurs when the *mobility edge* crosses the origin, as in Fig. 5.

-
- [1] J. D. Murray, *Mathematical Biology* (Springer-Verlag, N.Y., 1993).
 - [2] A. J. Koch and H. Meinhardt, Rev. Mod. Phys. **66**, 1481 (1994). See also Sec. XI of M.C. Cross and P.E. Hohenberg, Rev. Mod. Phys. **65** (1993).
 - [3] A recent exception is the numerical study of the effect of quenched randomness on Turing patterns in reaction-diffusion systems by I. Bose and I. Chaudhuri, cond-mat/9702230; see also M.W. Deem and J.M. Park, cond-mat/9707254.
 - [4] R. A. Fisher, Ann. Eugenics **7**, 353 (1937).
 - [5] A. Kolmogoroff, I. Petrovsky and N. Piscounoff, Moscow Univ. Bull. Math. **1**, 1 (1937).
 - [6] See, e.g. J.D. Gunton, M. San Miguel and P.S. Sahni, in *Phase Transition and Critical Phenomena*, vol. 8, edited by C. Domb and J. Liebowitz (Academic, New York, 1983).
 - [7] To see why $c(\mathbf{x}, t) \geq 0$, suppose $c(\mathbf{x}, t)$ is initially non-negative but about to pass through zero at a point \mathbf{x}_0 , i.e., $c(\mathbf{x}_0, t) = 0^+$ and $\frac{\partial c(\mathbf{x}_0, t)}{\partial t} < 0$. However, all terms in Eq. (1.2) except the Laplacian then vanish at this point. If $c(\mathbf{x}, t)$ is not *identically* zero in the vicinity of the point \mathbf{x}_0 , then \mathbf{x}_0 is a local minimum and $\frac{\partial c(\mathbf{x}_0, t)}{\partial t} = D \nabla^2 u(\mathbf{x}_0, t) > 0$ which contradicts the assumption that $\frac{\partial c(\mathbf{x}_0, t)}{\partial t} < 0$.
 - [8] C. H. Li and M. O. Robbins, Phys. Rev. **B46**, 14519 (1992).
 - [9] D. T. Natterman, S. Stepanow, L.-H. Tang and H. Leschom, J. Phys. (France) **II 2**, 1483 (1992).
 - [10] O. Narayan and D. S. Fisher, Phys. Rev. **B48**, 7030 (1993).
 - [11] G. Grinstein, Z.-W. Lai and D. A. Browne, Phys. Rev. **A40**, 4820 (1989). See also, M. A. Munoz and T. Hwa, cond-mat/9702217.
 - [12] It should be noted that we study here growth of *continuous* populations, while the actual process is certainly discrete — the spreading of a gene, as well as the change of the population, comes, of course, in quanta of one or more individuals, and are not continuous variables. Throughout this paper, we neglect this effect and study only the continuum process. Discreteness can be modeled by inclusion of a multiplicative Langevin noise term, see, e.g. V. Privman, Trends in Stat. Phys. **1** (1994); J. Cardy, cond-mat/9607163; J. Cardy and Uwe C. Täuber, cond-mat/9609151.
 - [13] J.-I. Wakita, K. Komatsu, A. Nakahara, T. Matsuyama and M. Matsushita, J. Phys. Soc. Japan, **63**, 1205 (1994).
 - [14] H. Berg, *Random Walks in Biology* (Princeton University Press, Princeton, New Jersey 1993).
 - [15] J. Miller and J. Wang, Phys. Rev. Lett. **76**, 1461 (1996); J.T. Chalker and J. Wang, cond-mat./9704198. See also D.S. Fisher, Phys. Rev. **A 30**, 960 (1984) and J.A. Aronovitz and D.R. Nelson, Phys. Rev. **A 30**, 1948 (1984).
 - [16] D. R. Nelson and P. Le Doussal, Phys. Rev. **B 42**, 10113 (1990); For a related treatment of convection of a passive scalar, see B. Shraiman and E.D. Siggia, Phys. Rev. **E49**, 2912 (1994).
 - [17] D.R. Nelson and V.M. Vinokur, Phys. Rev. **B 48**, 13060 (1993).
 - [18] D. Haarer and H. Mohrwald, Phys. Rev. Lett. **34**, 1447 (1975).
 - [19] B. Movaghar, G.W. Sauer and D. Wurtz, J. Stat. Phys. **27**, 473 (1982); B. Movaghar B. Pohlman and D. Wurtz, Phys. Rev. **A 29**, 1568 (1984).
 - [20] P. Grassberger and I. Procaccia, J. Chem. Phys. **77**, 6281 (1982); Phys. Rev. **A 26**, 3686 (1982).
 - [21] L. W. Chen, L. Balents, M.P.A. Fisher and M. C. Marchetti, Phys. Rev. **B54**, 12798 (1996).
 - [22] K. B. Efetov, Phys. Rev. Lett. **79**, 491 (1997), cond-mat/9702091; J. Feinberg and A. Zee, cond-mat/9703087; R. A. Janik, M. A. Nowak, G. Papp and I. Zahed, cond-mat/9705098; J. Feinberg and A. Zee/9706218; I. V. Goldsheid and B. A. Khoruzhenko, cond-mat/9707230; and Ref. [30].
 - [23] B. I. Shklovskii and A.L. Efros, *Electronic Properties of Doped Semiconductors* (Springer-Verlag, N.Y., 1984).
 - [24] A similar transformation has been used for Fokker-Planck equations by, e.g., P. G. de Gennes, J. Stat. Phys. **12**, 463 (1975); See also H. Risken, *The Fokker-Planck Equation* (Springer, Berlin, 1984) Chapter 5. For the application to localized states, see P. Le Doussal (unpublished), and Appendix A of Ref. [21].
 - [25] N. Hatano and D. R. Nelson, Phys. Rev. Lett. **77** 570 1996; N. Hatano and D. R. Nelson, cond-mat/9705290 (Phys. Rev. B, in press).
 - [26] D. Forster, D. R. Nelson and M. Stephen, Phys. Rev. **A16**, 732 (1977).
 - [27] See, e.g. G.B. Whitham, *Linear and Nonlinear Waves* (Wiley, New York, 1974), Chapter 4.
 - [28] See, e.g., F. R. Gantmacher, *The Theory of Matrices*, Chelsea Publishing Company, N.Y. (1974).
 - [29] K. G. Wilson and J. Kogut, Physics Reports, **12C**, 77 (1974).
 - [30] P.W. Brouwer, P.G. Silvestron and C.W.J. Beenakker, cond-mat/9705186.
 - [31] T. Hwa, D.R. Nelson and V. Vinokur, Phys. Rev. **B48**, 1167 (1993).
 - [32] N. Shnerb and D.R. Nelson, to be published.
 - [33] See, e.g., T. Halpin-Healy and Y. Zhang, Phys. Rep. **254**, 215 (1995); D. S. Fisher, in *Phase Transitions and Relaxation in Systems with Competing Energy Scales*, Edited

- by T. Riste and D. Sherrington (Kluwer, Boston 1993); and M. Kardar and Y.-C. Zhang, Phys. Rev. Lett. **58**, 2087 (1987).
- [34] For an analysis of sample-to-sample fluctuations in the growth spectrum in one dimension at intermediate values of v , see Ref. [30].
- [35] See, e.g. R. Shankar, *Principles of Quantum Mechanics*, (Plenum, New York, 1980).
- [36] L.-H. Tang, M. Kardar and D. Dhar, Phys. Rev. Lett. **74**, 920 (1995).
- [37] S. P. Obukhov, Physica **A 101**, 145 (1980)
- [38] See, e.g., R. Friedberg and J.M. Luttinger, Phys. Rev. **B 12** 4460 (1975).
- [39] For a numerical evaluation of the density of states in the one-dimensional lattice model, see T. Saso *et al.*, Prog. Theor. Phys. (Supplement) **84**, 269 (1985).